Geological Society of America
Special Paper 388
2005

Shear wave splitting around hotspots: Evidence for upwelling-related mantle flow?

Kristoffer T. Walker* **
Götz H.R. Bokelmann**
Simon L. Klemperer
Department of Geophysics, Stanford University
Andrew Nyblade
Department of Geosciences, Pennsylvania State University

ABSTRACT

We review evidence for plumelike upwellings beneath the Eifel, Great Basin, Hawaii, Afar, and Iceland hotspots by using teleseismic shear wave splitting to resolve the anisotropy associated with mantle flow. An approximately parabolic pattern of fast polarization azimuths (ϕ) is consistent with splitting observations around the Eifel, Great Basin, and Hawaii hotspots, and this pattern may be explained by a model of upwelling material that is being horizontally deflected or sheared in the direction of absolute plate motion (parabolic asthenospheric flow, PAF). The source of splitting beneath Iceland and the Afar is not clear, but the data are not inconsistent with a plumelike upwelling. The success of the upwelling model in explaining the splitting data for the Eifel and the Great Basin, regions far from plate boundaries, suggests that a mantle anisotropy pattern exists for at least some hotspots driven by plumelike upwellings and that splitting can be a useful diagnostic to differentiate between plumelike and alternative sources (e.g., propagating cracks, leaky transform faults) for mantle hotspots. Furthermore, the PAF pattern provides two useful tectonic and geodynamic parameters: the direction of relative motion between the lithosphere and asthenosphere and the stagnation distance, which is proportional to the strength of the upwelling and the speed of the moving plate. When this pattern is used with other types of geophysical data such as seismic velocity tomographic images, one can estimate the plate speed, upwelling volumetric flow rate, buoyancy flux, asthenospheric thickness, excess temperature, and viscosity.

Keywords: Eifel, anisotropy, plumes, shear wave splitting, geodynamics, tectonics

*E-mail: walker@ucsd.edu.
**Present addresses: Walker—Institute of Geophysics and Planetary Physics, Scripps Institution of Oceanography, University of California–San Diego; Bokelmann—Laboratoire de Tectonophysique, Université Montpellier II.

Walker, K.T., Bokelmann, G.H.R., Klemperer, S.L., and Nyblade, A., 2005, Shear wave splitting around hotspots: Evidence for upwelling-related mantle flow?, *in* Foulger, G.R., Natland, J.H., Presnall, D.C., and Anderson, D.L., eds., Plates, plumes, and paradigms: Geological Society of America Special Paper 388, p. 171–192, doi: 10.1130/2005.2388(11).

INTRODUCTION

The plate tectonics hypothesis, that rigid plates move over the Earth's surface above a fluidlike mantle, explains most of Earth's geological and geophysical features (Dietz, 1961; Hess, 1962). Some of the most prominent features that are not easily explained by plate tectonics are "hotspots," anomalous volcanic regions far from plate boundaries (e.g., Hawaii and Yellowstone) that are often associated with some combination of rapid and voluminous eruptions of basaltic lava, broad topographic swells and geoid highs, and linear age progressions of volcanic centers (e.g., Morgan, 1971; Courtillot et al., 2003). These are, in contrast, often explained by the plume hypothesis—that cylindrical conduits of hot upwelling mantle material are responsible for ~10% of Earth's heatflow (Sleep, 1990; Davies and Richards, 1992). Recently the plume hypothesis has been challenged, and plate tectonic models have been proposed instead to explain such regions (e.g., Anderson, 1994; King and Anderson, 1998; Smith and Lewis, 1999).

The existence of plumes is difficult to establish with seismological data because of their hypothesized geometry and depth. Typical regional tomographic inversions of teleseismic body wave data, which suffer from the inherent tradeoff between misfit reduction and model complexity, tend to smear anomalies vertically in regions penetrated by mostly subvertical rays. Consequently applications of this technique around hotspots (e.g., Bijwaard and Spakman, 1999; Foulger et al., 2001; Wolfe et al., 2002) have led to intriguing but sometimes controversial image interpretations. In addition, resolution constraints and choice of reference velocity in past global and regional inversions have limited detailed imaging of the deep lower mantle beneath hotspots (Ritsema and Allen, 2003).

Although recently there has been success in providing seismological evidence for some plumelike structures with surface wave anisotropy tomography (Montagner and Guillot, 2000), finite-frequency body wave tomography (Montelli et al., 2004), and SS precursors and receiver functions (Li et al., 2003), new approaches for detecting plumes will help resolve the controversy. For example, seismic velocity anisotropy in the upper mantle can be detected by teleseismic shear wave splitting (Fig. 1), i.e., the separation of the shear wave in the anisotropic upper mantle into two waves, polarized in mutually orthogonal orientations, traveling at different speeds to the seismic station. The accumulated splitting delay time (*dt*) is proportional to the product of the magnitude of anisotropy and the length of the ray path through the anisotropic medium, with typical teleseismic *dt* of 0.3–2.0 s. Therefore, constraining the depth of anisotropy from shear wave splitting can be difficult. However, correlations of increasing *dt* with increasing lithospheric thickness (Silver, 1996), in splitting from SKS and local S phases (Fischer and Wiens, 1996), and in splitting direction and surface wave anisotropy in oceanic and young continental regions (Montagner and Guillot, 2000) suggest that the upper 300 km of the mantle is anisotropic and the dominant source of teleseismic splitting.

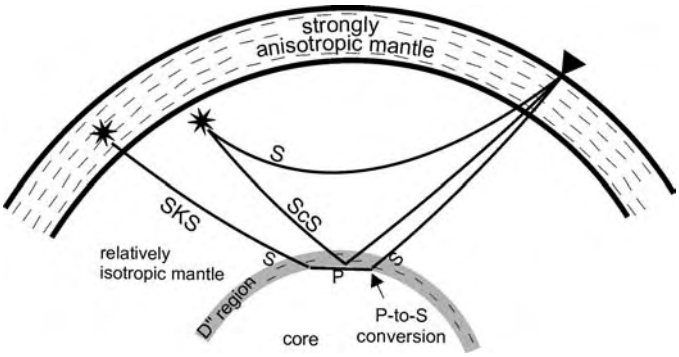

Figure 1. The geometry of teleseismic shear wave splitting. Shear phases (e.g., SKS, ScS, and S), generated by earthquakes (stars), experience shear wave splitting while propagating upward through the mantle almost directly beneath the seismic station (triangle). Core-refracted phases obtain a radial polarization (in the earthquake-station plane) during a P-to-S conversion upon exiting the liquid outer core, while S and ScS phases obtain their initial polarization at the source. The dominant source of shear wave splitting is most likely the anisotropy 0–300 km beneath the seismic station.

This anisotropy can be explained by a lattice preferred orientation of olivine fast a-axes due to either past or present mantle deformation via dislocation creep (Fig. 2). This splitting interpretation has been used to explain correlations of fast polarization azimuth (ϕ) with absolute plate motion (Vinnik et al., 1992; Bormann et al., 1996; Schutt and Humphreys, 2001), although many other interpretations have been proposed to explain other correlations (Fig. 3; Savage, 1999). We defer more detailed discussion of the relationships among olivine, deformation, anisotropy, and splitting to review papers published elsewhere (e.g., Savage, 1999).

An essential prediction of the plume hypothesis in the presence of mobile plates is the deflection of buoyant, actively upwelling plume material leading to an approximately parabolic subhorizontal flow pattern in map view (Fig. 4). This prediction may be tested by analyzing shear wave splitting of shear phases generated from teleseismic earthquakes (Savage and Sheehan, 2000; Walker, 2004). The ability to resolve this deflection depends on the volumetric flow rate, asthenospheric thickness, plate speed, spatial extent of the seismic array, and existence of additional anisotropy that could complicate or mask a plume signal. Widely spaced arrays on fast-moving plates above weak upwellings and a thick asthenosphere will not be capable of resolving this deflection, and they will detect the asthenospheric flow only in the direction of plate motion. Narrow arrays on slow-moving plates above vigorous upwellings and a thin asthenosphere will detect the deflection, but it will be in a radial pattern originating from the hotspot. Between these two end-member models is a spectrum of different parabolic asthenospheric flow (PAF) models. These models have been described kinematically by Sleep (1987), Richards et al. (1988), and Olson (1990). Subsequent numerical modeling (Ribe and Christensen, 1994, 1999)

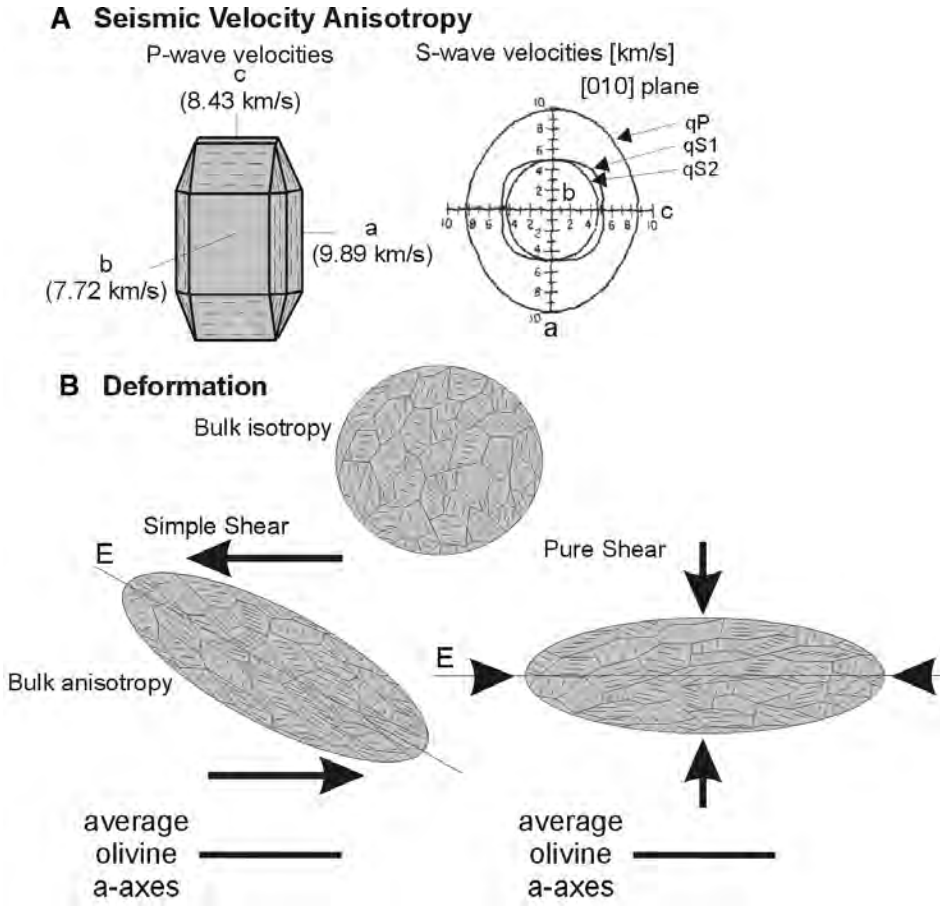

Figure 2. Relationship between seismic anisotropy and dislocation creep deformation for olivine in anhydrous conditions. (A) For a single crystal of olivine, the fast a-axis and slow b-axis give rise to a maximum P-wave and S-wave anisotropy of ~25% and 12% (modified from Nicolas and Christensen, 1987). Abbreviations: qP—quasi-P; qS1—quasi-S1 (fast); qS2—quasi-S2 (slow). (B) A dunite comprised of randomly oriented grains of olivine has an average or bulk isotropy. Progressive pure shear or simple shear deformation of the same rock via dislocation creep will create a lattice preferred orientation (LPO) of fast olivine a-axes in the direction of shear (simple shear) or elongation (pure shear), leading to an elongation along line E and a bulk anisotropy (Nicolas and Christensen, 1987). The dark line beneath each deformed sample represents the flow direction and LPO of olivine fast a-axes. This line is a proxy for the shear wavesplitting fast polarization azimuth (ϕ) and delay time (*dt*) that would be observed for a shear wave. Lab and field studies confirm that LPO S-wave anisotropy of dunites can be at least as large as 4% (Mainprice and Silver, 1993). Under water-rich conditions, the intermediate c-axis can become subparallel to the shear plane, and the fast a-axis subparallel to the pole of the shear plane (e.g., Jung and Karato, 2001).

has confirmed that the kinematic models are a good approximation for the horizontal flow directions near the conduit, but the kinematic pattern is wider than that provided by the numerical modeling far downstream from the conduit.

Because mantle anisotropy from a plume may be mostly confined to the upper 300 km of the Earth's mantle, an observed PAF pattern can suggest only the top of a "plumelike" upwelling, but not necessarily a plume defined in the strictest sense as originating from the lower mantle (e.g., Morgan, 1971). Furthermore, depending on the complexity of mantle flow and rheology, it is not clear if an upwelling interpreted from an observed PAF pattern must be an active upwelling or if it can also be passive in nature.

In this chapter we review and discuss the results of shear wave splitting around the Eifel, Hawaii, Iceland, and Afar hotspots and the Great Basin, which has some of the characteristics of a hotspot and is referred to as such for convenience. The Eifel results are relatively new, and we refer the reader to Walker (2004) for more detail regarding the data analysis, modeling, and tectonic/geodynamic parameter calculations. We show that the splitting data for the Eifel and the Great Basin uniquely predict a simple plumelike upwelling. Data from around Hawaii are consistent with such an upwelling, but do not predict one uniquely. The splitting data from Iceland and the Afar, hotspots bisected by spreading ridges, are more difficult to interpret, and permissible models include a mantle upwelling interacting with the spreading plates and basal lithospheric topography, aligned magma-filled lenses, and fossilized lithospheric anisotropy from past orogenic events. We compare the model parameters derived from the splitting data for the Eifel and the Great Basin to parameters for Hawaii estimated by rigorous finite-difference flow modeling. We also calculate the volumetric flow rates for each upwelling and calculate the Eurasian plate speed in a fixed hotspot reference frame. We then discuss the implications of these data in terms of the plume hypothesis, and we mention those hotspots for which there is forthcoming data as well as some avenues of future research.

EIFEL HOTSPOT

A vertically oriented anomaly of low compressional- and shear- (P- and S-)seismic velocity was imaged in the mantle (Ritter et al., 2001; Keyser et al., 2002) down to the 400 km depth limit of resolution beneath the 1997–1998 Eifel Plume Project Seismic Network, a dense network comprising 158 mobile seismic stations centered on the Eifel hotspot in west central

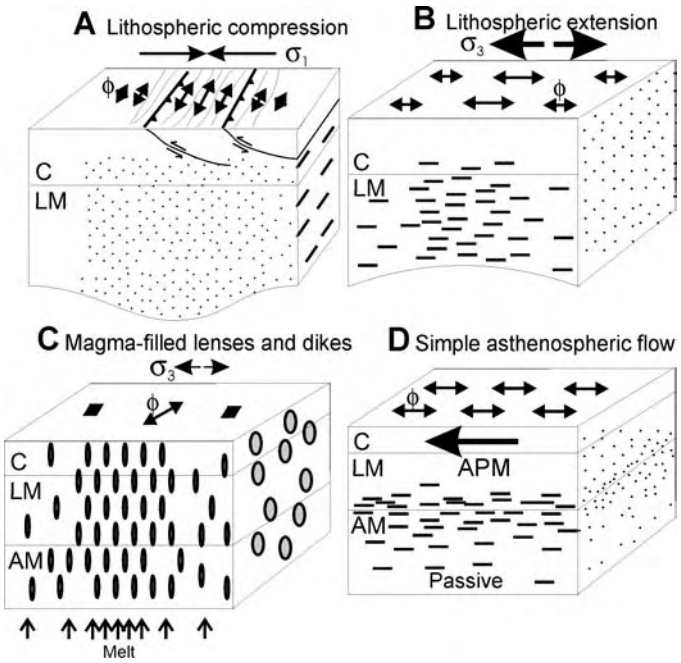

Figure 3. Different models that can produce shear wave splitting. Line orientation and length indicate the fast polarization azimuth (ϕ) and relative delay time (*dt*). Abbreviations: σ_1—maximum compression direction; σ_3—minimum compression direction; C—crust; LM—lithospheric mantle; AM—asthenospheric mantle. (A) Pure shear deformation via dislocation creep leads to a lattice preferred orientation (LPO) of olivine fast a-axes perpendicular to the direction of compression (parallel to the strike of the orogeny). (B) Lithospheric stretching induces an LPO of olivine fast a-axes in the direction of extension. (C) A shape preferred orientation (SPO) of aligned magma-filled lenses or dikes can develop in the presence of partial melt in a normal-faulting stress state, leading to effective anisotropy with ϕ perpendicular to the least compressive stress direction (parallel to the strike of the structures). The magnitude of this SPO anisotropy depends on the density of lenses or dikes, velocity contrast, aspect ratio, and scale of the lenses or dikes with respect to the dominant seismic wavelength. (D) Simple shear due to the relative motion between the moving plate and underlying mantle can lead to an LPO of olivine fast a-axes and ϕ in the direction of the vector difference of the two velocities. In the special case in which the plate speed is much faster than that of the underlying mantle, simple asthenospheric flow will develop, and ϕ will be oriented in the direction of absolute plate motion (APM).

Europe (Ritter et al., 2000). Receiver functions also resolve a depression of the 410 km discontinuity (Grunewald et al., 2001; M. Budweg, 2003, personal commun.). We analyze shear wave splitting in seismograms recorded during the seven-month operation of the Eifel Network, and we compare the observed fast polarization azimuths to those predicted for a simple upwelling.

Eifel Data

During the seven-month deployment of the Eifel Network, several core-refracted SKS phases were recorded. However, only two of these events are analyzed because they were of high quality, with an energy signal-to-noise ratio greater than 20. We used the method of Silver and Chan (1991) to make apparent splitting measurements and associated errors by filtering the waveforms with a 0.2 Hz low-pass filter, then performing a grid search over ϕ and *dt* to minimize the eigenvalue of the trial fast-slow covariance matrix. Figure 5 shows an example of splitting at permanent station WLF (for location see Fig. 6). We also analyzed up to fifteen years of recorded data on permanent seismic stations throughout west central Europe. These permanent stations afforded us the possibility of testing between different models of mantle anisotropy: single layer with a horizontal fast axis, single layer with a dipping fast axis, or two layers with horizontal fast axes. In general, we found that the best-fit models for both the dipping-axis and the two-layer case fit the data at each station marginally better than the single-layer models, but that the minor improvement in fit does not justify the inclusion of extra model parameters. In addition, these best-fit dipping-axis or two-layer models for stations that are relatively close together are very different, and the misfit functions used to find them have many local minima. Because the single-layer model has only one local minimum and because these models are very similar for stations that are relatively close together, we prefer the single-layer model to estimate the first-order anisotropy signal beneath the study area.

Figure 6 shows the single-layer splitting ϕ in the Eifel region of west central Europe (white bars). Numerous "null" stations did not demonstrate any splitting (white crosses), and this can be interpreted as showing that there is no anisotropy beneath the station, or that the fast axis of anisotropy (assuming a single layer) is parallel or perpendicular to the back azimuth. The back azimuth of the two Eifel SKS events (~70° and ~250°) are ~180° apart. Because some null stations occur between nearby constrained stations that have a ϕ subparallel to the back azimuth, the nulls likely indicate that there is anisotropy beneath those stations with a ϕ of ~70°.

Eifel Interpretation

A semicircular pattern of ϕ exists around the Eifel hotspot (Fig. 6). This spatial pattern, the high signal-to-noise ratio of the analyzed waveforms, and the small 95% error bars (average < 20°) on these models argue against this rotation as resulting from noise (Fig. 7). Many lines of evidence suggest that the lithosphere beneath the Eifel region is only 50–70 km thick (e.g., Babuska and Plomerová, 1993). The ϕ variation and the $dt > 0.4$ s cannot be explained by a single layer of fossilized lattice preferred orientation anisotropy within the lithosphere that is parallel to the 70° strike of the Hercynian orogeny, an interpretation that explains many of the ϕ beneath Europe's permanent broadband stations (Bormann et al., 1993; Silver, 1996). In addition, whereas the northwest-oriented ϕ to the northeast of the Eifel could be explained by vertically oriented lenses (Crampin, 1991; Kendall, 1994; Gao et al., 1997) that have formed in the lithosphere and the asthenosphere perpendicular to the northeast minimum horizontal compressive stress orientation, it is difficult to explain the range of other azimuths with such a model when the minimum

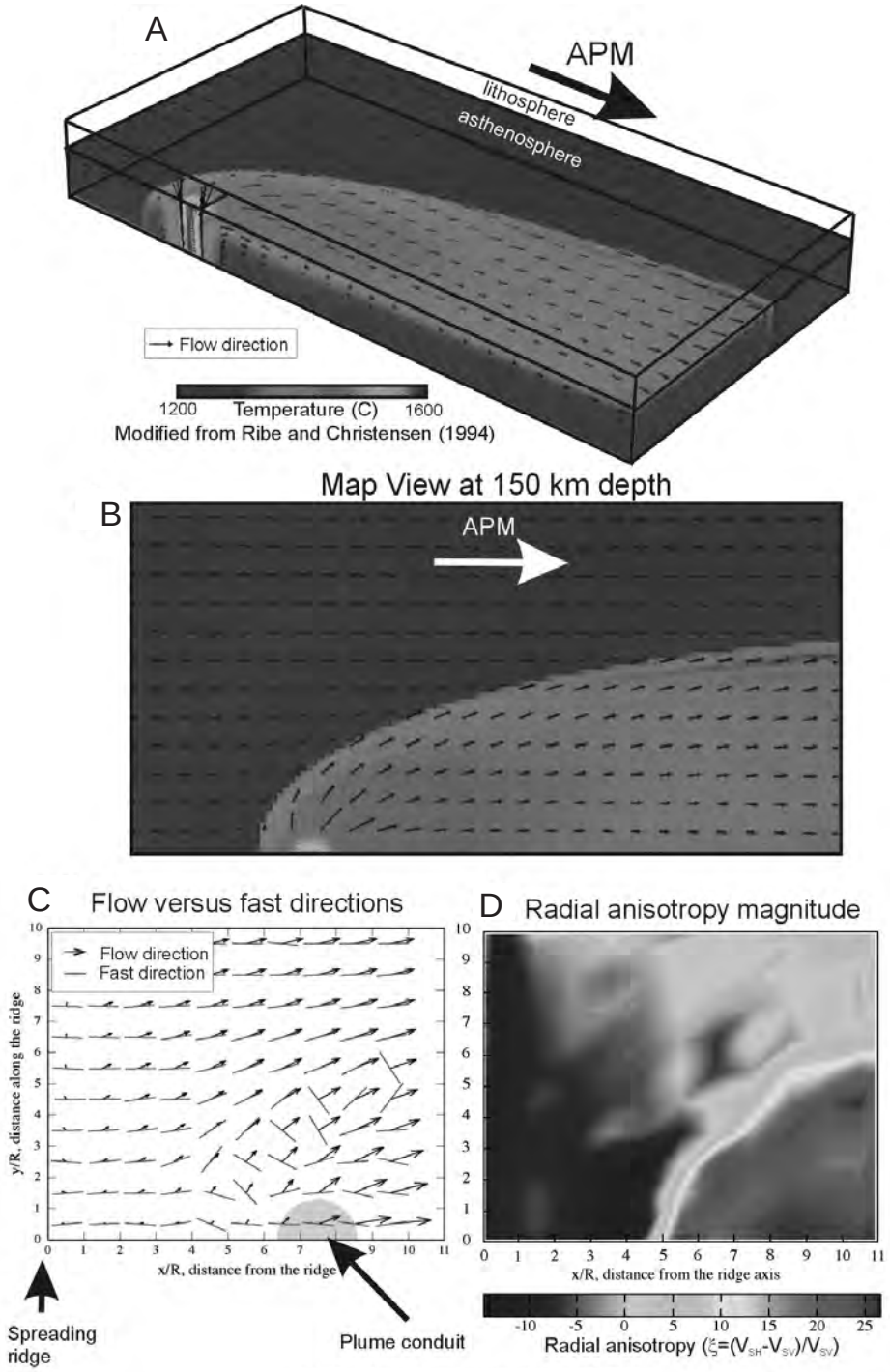

Figure 4. Geodynamic modeling results relevant to predicting upper-mantle anisotropy associated with upwellings. Panels A and B show the predicted asthenospheric flow pattern expected for a fixed mantle upwelling interacting with a moving plate (in this case for Hawaii beneath the Pacific plate; modified from Ribe and Christensen, 1994). The upwelling material impinges upon the plate, then spreads laterally into the asthenosphere, during which it is sheared in the direction of absolute plate motion (APM), leading to approximately parabolic mantle flow in map view. Panels C and D show the results of olivine lattice preferred orientation (LPO) modeling, assuming that both dislocation creep and dynamic recrystallization are important LPO generation and preservation processes, for a spreading ridge and an upwelling of radius R at a depth of 0.5R beneath a moving plate (modified from Kaminski and Ribe, 2002). The flow and fast directions in panel C may be subparallel at some distance from an upwelling, but are not generally subparallel in the proximity of the conduit. The color scale in panel D is the magnitude of radial anisotropy ($\xi = (V_{sh} - V_{sv})/V_{sv}$, where V_{sh} and V_{sv} are the S-wave velocities for horizontally and vertically polarized waves, respectively), which is expected to be strongly positive near the conduit. Different mantle viscosities can lead to different flow-modeling results; for example, small-scale convective features may be present if the asthenospheric viscosity is smaller.

stress orientation remains relatively constant throughout the area (Sperner et al., 2003).

Hence our interpretation is that the splitting data resolve a lattice preferred orientation of olivine associated with active mantle deformation of the asthenosphere, which begins at a depth of ~60 km beneath the Rhenish massif (e.g., Babuska and Plomerová, 1993). This interpretation is somewhat consistent with the results of Becker et al. (2003) for our study area, which show evidence that the largest axis of the finite strain ellipsoid in the asthenosphere from global tomography-based geodynamic flow models (which have a relatively poor spatial resolution) is between northeast-southwest and northwest-southeast down to

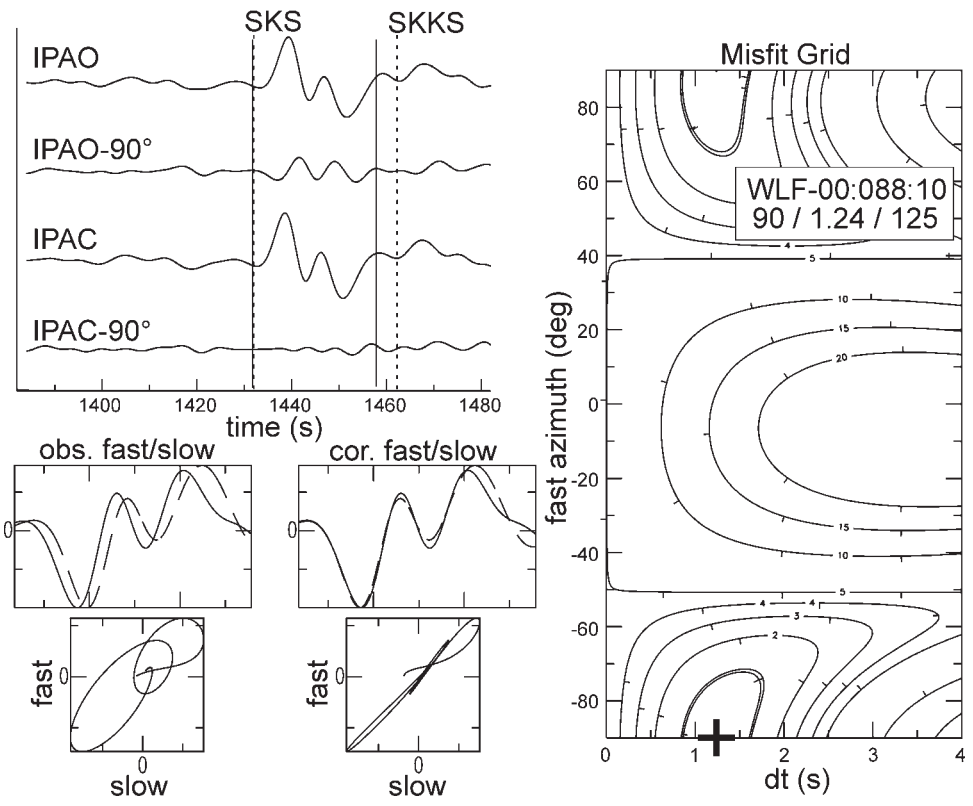

Figure 5. Shear wave splitting example for station WLF (for location, see Fig. 6). We use the method of Silver and Chan (1991) as modified by Walker (2004) to find the optimum fast polarization azimuth (ϕ) and delay time (*dt*) by performing a grid search (right) over ϕ and *dt* to minimize coherent energy on the anisotropy-corrected component that is perpendicular to the initial polarization azimuth (left; IPAC-90°), which is equivalent to maximizing the linearity of horizontal particle motion (lower left). The four diagrams at lower left show the observed and *dt*-corrected fast and slow waves and corresponding particle motions for the time window in the diagram at upper left. *Upper right:* The date and time of the analyzed event (year:julday:hour), the measured ϕ and *dt*, and the energy signal-to-noise ratio.

400 km depth, the average of which is subparallel to the average ϕ observed throughout the study region.

In light of this interpretation, it makes sense to test the plumelike upwelling hypothesis. We do this by using a hydrodynamical streaming potential function (Milne-Thomson, 1968) to estimate the orientations of the flow lines expected for a vertical conduit feeding upwelling material into a tabular horizontal stream (the top of the asthenosphere). Assuming that the deformation is occurring partly via dislocation creep and that the fast wavespeed directions are approximately parallel to the flow directions, we perform a grid search using ϕ from constrained-station estimates over the four model parameters: upwelling center latitude and longitude, parabolic width (stagnation distance), and pattern opening direction (background asthenospheric flow relative to a fixed hotspot reference frame). If the asthenosphere passively deforms due to plate motion, the background asthenospheric flow direction is parallel to absolute plate motion. The stagnation streamline is the imaginary line that separates the normal asthenosphere from the horizontally spreading upwelling material at the base of the lithosphere (Sleep, 1987). The distance from the conduit upstream to this line is the stagnation distance, $r_s = u/sh$, where u is the volumetric flow rate, s is the plate motion speed, and h is the thickness of the low-viscosity asthenosphere into which the upwelling laterally spreads. This model is computationally efficient to compute. However, it is crude in that it is purely kinematic, does not account for variable viscosities and deformation mechanisms, and does not account for the possibility of small-scale convection.

The optimum Eifel PAF model and 95% confidence limits were derived from a bootstrap method (Table 1). This model explains 61% of the variation in ϕ from the 70° mean and has a stagnation distance of r_s = 60 km (Fig. 8). Approximately the same model is recovered if we include the null stations in our grid search and use several different grid-search optimization techniques. An incremental F-test demonstrates that the PAF model (four model parameters) explains the data statistically better than a unidirectional model with a ϕ of 70°. Inspection of the marginal misfit functions, random sampling of the misfit space (4D histogram projections), and 2D plots of local minima clearly confirm that the optimum PAF model is well constrained and uniquely predicted by the data (Fig. 9).

The obvious second-order variation (39% not fit by the PAF model) is interpreted to be due to a combination of data error and model error. The data error will decrease in time after more splitting data have been collected and analyzed around the Eifel hotspot; however, we interpret the model error to be due to several possible factors. As mentioned earlier, the lithosphere beneath the Eifel region is only 50–70 km thick. Inspecting the Fresnel zone for an SKS phase arriving at two stations separated by 50 km suggests that there is no significant overlap above ~100 km depth (Alsina and Snieder, 1995; Wylegalla et al., 1999). If anisotropy is purely single-layer, this suggests that

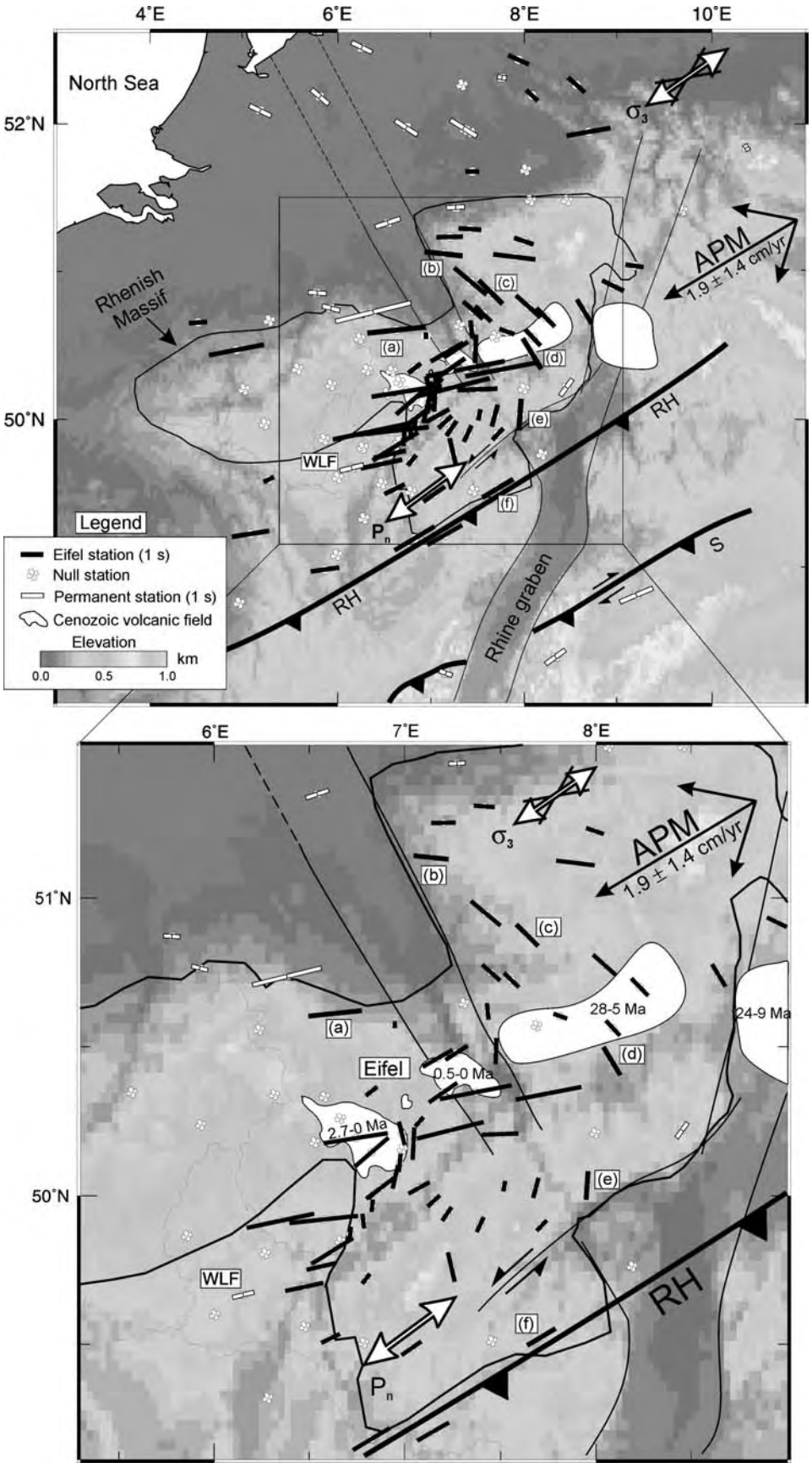

Figure 6. Shear wave splitting results for the study area and the Eifel region. Lines—station splitting estimates, with orientation parallel to fast polarization azimuth and length proportional to delay time. White crosses—stations for which no splitting was observed (null stations). Measurements at stations a–f are presented in Figure 7. Thick contour—boundary of uplifted Rhenish Massif. Black lines with hatch marks—Cenozoic rift system including the Rhine graben in the south, the Rut graben in the northwest, and the Leine graben in the northeast. Thick lines—deep-seated reverse and wrench faults that separate Hercynian orogeny terranes (RH—Rhenohercynian and S—Saxothuringian sutures; Edel and Fluck, 1989). White bodies—volcanic centers with their ages in Ma (R—Recent) (Illies et al., 1979; Jung and Hoernes, 2000). Double-headed arrow in the south—P_n-velocity fast orientation (Smith and Ekström, 1999). Double-headed arrow in the north—regional average least horizontal compressive stress direction (σ_3) (Mueller et al., 1997). Black vector—absolute plate motion (APM) and 2σ error bars in a fixed hotspot reference frame (Gripp and Gordon, 2002).

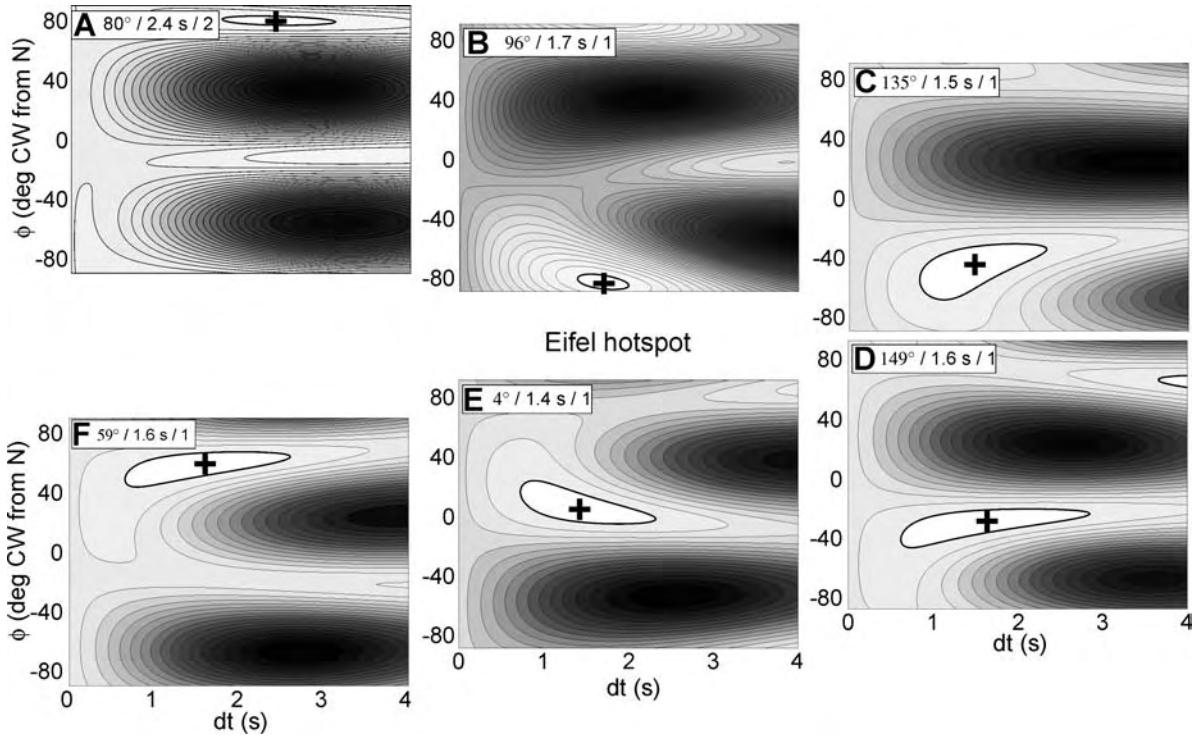

Figure 7. Examples of station splitting estimates for stations a-f (for location, see Fig. 6) showing a rotation of fast polarization azimuth (ϕ) around the Eifel hotspot. White boxes give the station name, splitting parameters, and number of events analyzed; *dt*—delay time. The optimum splitting parameters are indicated by the global minima (pluses) of the misfit grids. The 95% confidence region is indicated in white.

changes in splitting could be observed only due to a lateral variation of anisotropy in a layer above ~100 km depth. For a two-layer model, the splitting that occurs in the upper layer has the most effect on the total apparent splitting (e.g., Rümpker and Silver, 1998; Saltzer et al., 2000). It is therefore also possible to explain rapid lateral variations in apparent splitting by a combination of uniform or slowly varying anisotropy below and rapidly varying anisotropy above ~100 km depth. We speculate that the remaining 39% variation not fit by the PAF pattern is due to subregions of additional lithosphere and asthenosphere anisotropy associated with fossilized olivine fabrics, magma-filled lenses, strong active deformation near the base of the plate associated with flow complexities (e.g., small-scale convection), or the effects of dynamic recrystallization (Fig. 4C; Kaminski and Ribe, 2002). Using additional techniques and data to unambiguously locate the depth distribution of anisotropy beneath the Eifel will of course help distinguish which of these possible phenomena, if any, are responsible for the second-order variation.

Figure 10 shows the flow lines from the PAF pattern and our station splitting estimates superimposed on a map of shear wave velocity between 100 and 170 km depth (Keyser et al., 2002). For most of the data, *dt* = 1.0–1.5 s. However, the constrained *dt* in and close to the Quaternary Eifel volcanic fields are anomalously large (~2–3.5 s). These large *dt* near the predicted upwelling center may suggest strong anisotropy in the asthenosphere, which has been predicted just downstream of conduits by modeling the development of the lattice preferred orientation of olivine associated with the deflection of upwelling plume material by a moving plate (Kaminski and Ribe, 2002; Fig. 4). However, because the modeled lattice preferred orientation varies dramatically in three dimensions, one must forward-model the observed splitting before a valid comparison can be made (e.g., Tommasi, 1998; Rümpker et al., 1999, 2003). Nonetheless, if splitting above the hotspot is due to anisotropy in the conduit, the olivine fast a-axes are probably not vertical (Rümpker and Silver, 2000), and this may suggest the presence of water (Jung and Karato, 2001; Karato, 2003). Varying water content has already been invoked for the Eifel upwelling to explain the discrepancy between P- and S-velocity anomalies (Keyser et al., 2002).

The large *dt* may also be a result of a lack of ability to resolve splitting because ϕ is roughly parallel to the back azimuths of the two SKS phases. The threshold of splitting resolution (the deviation between ϕ and back azimuth below which splitting is not reliably detected) depends on two factors: the signal bandwidth and the signal-to-noise ratio. The higher these two factors are, the lower the threshold. The data have a high signal-to-noise ratio, but the bandwidth is only fair (between 0.02 and 0.2 Hz). However, although the null measurements clearly do not have significant energy on their transverse components, the

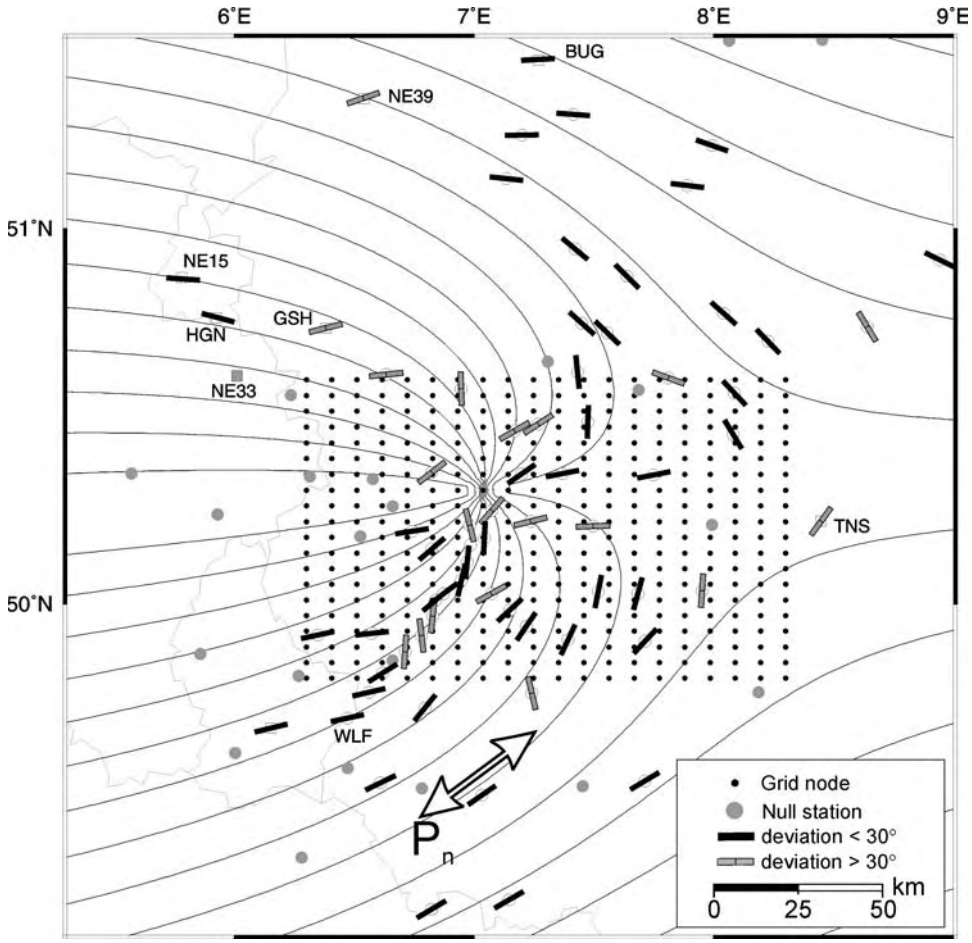

Figure 8. Testing the parabolic asthenospheric flow (PAF) model for the Eifel hotspot. The lines indicate the station splitting estimates normalized to a uniform delay time because the PAF pattern we test is only kinematic. The gray circles indicate null stations. The black dots show the plume-center search grid (Ritter et al., 2001; Keyser et al., 2002) while maintaining a twenty-node sampling in both X and Y directions. The black curves are the asthenospheric horizontal flow lines of the optimum PAF model, which predict 61% of the spatial variations in fast polarization azimuth.

measurements with large *dt* have a significant amount of transverse energy that is well attenuated after correction using the optimum splitting parameters. Given the facts that these *dt* are some of the largest observed anywhere in the world for SKS phases and that in some places our splitting parameters change remarkably over short spatial distances, we prefer to present the PAF pattern as a first-order pattern for the study region, recognizing that anisotropy is likely to be more complex. Of course more data need to be collected before the level of this complexity can be reliably ascertained.

Our PAF pattern has interesting consistencies with other results. The most obvious consistency is that our optimum conduit location from the grid search is at the center of the low-velocity anomaly between 100 and 170 km depth and between the two most recently active Eifel volcanic fields (Fig. 10). In addition, with respect to all directions from 0 to 360°, the optimum background asthenospheric flow direction of 260 ± 20° is consistent (within 2σ uncertainties) with the HS3-NUVEL1A absolute plate motion direction of 239 ± 44° (Gripp and Gordon, 2002) and with the average direction (~270°) of fast olivine a-axes inferred from a magnetotelluric investigation that documents a directional dependence on conductivity for asthenospheric depths below 70–90 km across the region (Leibecker et al., 2002). This suggests that the PAF pattern is due to a plumelike upwelling beneath the hotspot and that asthenospheric flow beneath the Eifel is a passive response to plate motion. A 410 km discontinuity deflection (Grunewald et al., 2001) and the depth extent of the low P- and S-velocity anomalies (Ritter et al., 2001; Keyser et al., 2002) suggest that the upwelling originates from at least 400 km beneath the Eifel. In fact, a large part of the low P-velocity anomaly beneath the Eifel, albeit not resolved as well as the main anomaly beneath the center of the Eifel Network, plunges toward the northeast as would be expected for a plate dragging upwelling material toward the southwest.

Eurasian Plate Speed Estimation

Resolving the plate motion of Eurasia with respect to a fixed hotspot reference frame has been challenging. The success of the PAF model in explaining the data allows us to put a constraint on absolute plate motion. If we assume that the vertical thickness of plume material spreading beneath the plate is the same beneath the Eifel and Hawaii, and if we use the Eifel excess upwelling temperature of 100–150 K and the conduit radius

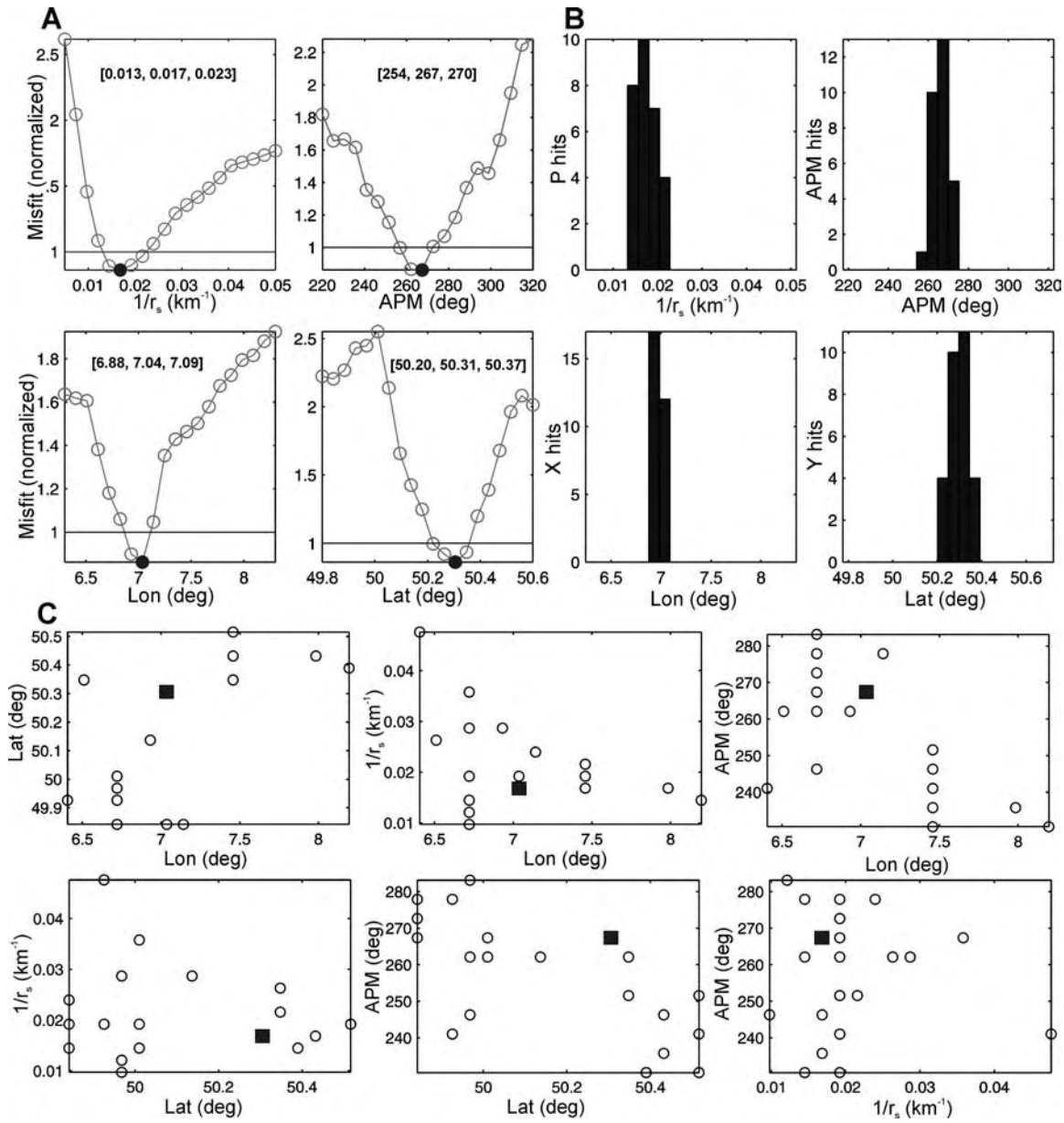

Figure 9. The resolution of the optimum parabolic asthenospheric flow (PAF) model. We searched for the optimum PAF model parameters that best explain the observed fast polarization azimuths. The model parameters are the latitude and longitude of the plume center, the stagnation distance (P), and the absolute plate motion direction (APM). (A) The marginal misfit curves showing the optimum model (solid circle) and the 95% confidence region as defined by the region beneath the horizontal line. The numbers in brackets are minimum, optimum, and maximum values for each parameter. (B) The histograms of the results of randomly targeting nodes in the misfit grid and testing whether they are below the 95% confidence contour. (C) 2D projections of the locations of local minima that are not possible solutions at the 2σ confidence level (circles) showing the optimum solution (square). These plots indicate that the optimum model is well resolved.

of 50–60 km estimated from the tomographic data (Ritter, 2005), mantle rheological parameters from Karato and Wu (1993), and geodynamic plume parameters for Hawaii (Ribe and Christensen, 1999), we calculate a Eurasian plate speed of 12 mm/a, which is within the 95% confidence limits of the 19 ± 14 mm/a Eurasian absolute plate motion of Gripp and Gordon (2002). The 2.7 Ma west Eifel and recently active east Eifel volcanic fields, which are aligned in an approximately northeast-southwest orientation (Fig. 10), are separated by 65 km, which may indicate a recent Eifel volcanic center propagation rate of 24 mm/a. In summary, the PAF pattern for the Eifel and other types of geological and geophysical data suggest to us that since the

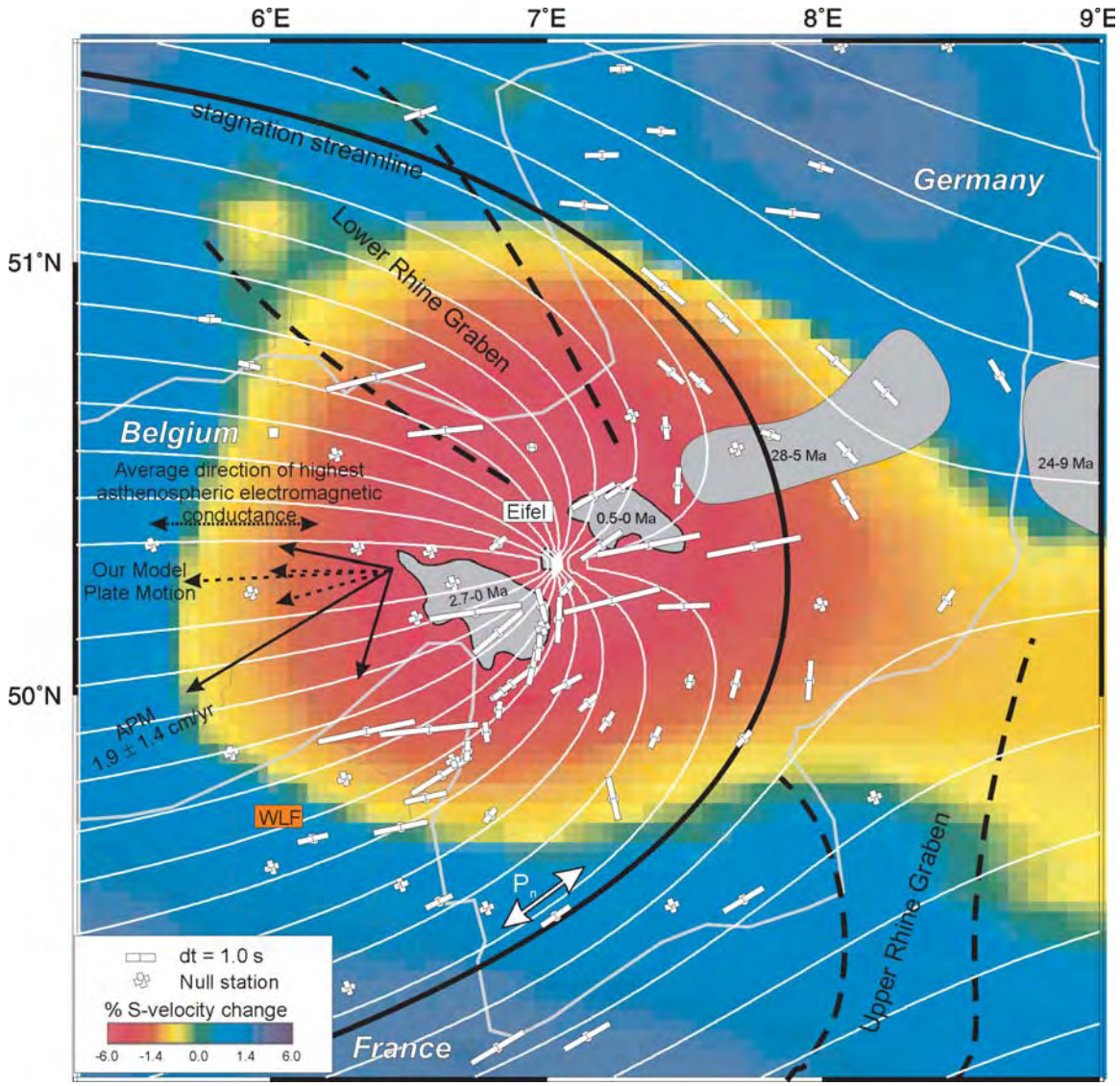

Figure 10. Splitting results across the Eifel hotspot in west central Europe. The short white lines are the teleseismic station splitting estimates, with length proportional to delay time. The background tomographic map indicates relative seismic S-velocity between 100 and 170 km depth (Keyser et al., 2002). The black lines are flow lines of our optimum parabolic asthenospheric flow model. This model has a stagnation distance of 60 km (Table 1). APM—absolute plate motion.

Late Pliocene, the absolute Eurasia plate motion has been on the order of 10–30 mm/a in the west-southwest direction.

Eifel Plume or Plumelike Upwelling?

It is interesting to note that there is no pre–Late Pliocene linear volcanic age progression or recognizable flood basalts associated with the Eifel hotspot. If the plate motion did not change significantly in the Pliocene, this hotspot is not similar to those that can be explained by the classic plume model. Courtillot et al. (2003) reviewed the current debate regarding the origin of mantle hotspots. They argue that many global topographic, geologic, geophysical, and geochemical data can be explained by three different sources for hotspots: plumes from the core-mantle boundary (e.g., Morgan, 1972), plumelike upwellings from the transition zone (e.g., Montagner, 1994; Allegre, 2002), and upper-mantle features related to lithospheric extension (e.g., Anderson, 2000). It now appears that the Eifel hotspot has a topographic, P-velocity (Ritter et al., 2001), S-velocity (Keyser et al., 2002), Q (Meyer, 2001), receiver function (Grunewald et al., 2001), geochemical (Wilson and Patterson, 2001), and mantle anisotropy anomaly that suggests a plumelike source. However, this upwelling is most likely weak and has a low excess temperature. This explains the lack of major continuous volcanism and a

recognizable hotspot track. Our preferred model is that the source of the Eifel plumelike upwelling is a fluctuating temperature and perhaps compositional perturbation, perhaps along a boundary layer in the mantle transition zone. This view is consistent with the receiver function study across the Eifel (Grunewald et al., 2001), which suggests anomalously hot material in the vicinity of the deflected 410 km discontinuity, but none associated with the unmodified 660 km discontinuity. Although global images from Bijwaard et al. (1998) have been presented by Goes et al. (1999) as evidence for a lower-mantle source of Eifel volcanism, the more recent global tomographic results of Montelli et al. (2004) show only an upper-mantle velocity anomaly beneath the Eifel hotspot.

OTHER HOTSPOTS

Great Basin

Savage and Sheehan (2000) and Savage (2002) made measurements of teleseismic shear wave splitting throughout the Basin and Range in the western United States. They observed a semicircular pattern of ϕ surrounding a region in central and eastern Nevada, a region that is characterized by mostly null splitting measurements. They showed that a PAF model with a conduit centered beneath the null region explains the majority of the ϕ variation.

Walker et al. (2004b) made splitting measurements for six seismic stations along the Snake River Plain, Idaho (Fig. 11). After considering two-layer and dipping-axis anisotropy models, they found that a single layer of anisotropy with a horizontal fast axis was sufficient to explain the splitting measurements. They found a pattern in their single-layer station splitting models where ϕ rotates ~30° clockwise from the northeast to the southwest part of the Snake River Plain, then possibly back ~20° toward the northwestern Snake River Plain. After considering several mechanisms to explain these data as well as splitting observations along a transect that crosses the eastern Snake River Plain (Schutt et al., 1998), they found that the Savage and Sheehan (2000) PAF pattern simultaneously explained all the ϕ, but that the on-axis reduction in *dt* imparted from the PAF anisotropy can be explained by the effects of aligned magma-filled lenses in the partially molten region above.

As with the Eifel data, we performed a grid search (Fig. 11) over the four model parameters of the PAF pattern for all the data, excluding those from California, and refined the PAF model of Savage and Sheehan (2000). Specifically we found that the optimum model opens in the direction of absolute plate motion, with a stagnation distance of r_s = 180 km, and is centered at the edge of the 2.0 km topographic bulge in eastern Nevada (Table 1). This pattern is uniquely determined at the 95% confidence level, and it fits 64% of the variation from the average ϕ orientation, which is a slightly better fit than that for the Eifel hotspot (61%).

Splitting ϕ in California are not explained by the downstream component of this PAF model. This may be due to regional effects of shearing along the San Andreas fault zone (e.g., Silver and Savage, 1994), a local downwelling beneath California associated with the recently subducted Farallon slab (e.g., Schmid et al., 2002), and/or the relative motion between the northwest-moving California and an eastward-moving sub-asthenospheric flow in a fixed hotspot reference frame (Silver and Holt, 2002).

The existence of an upwelling beneath eastern Nevada is consistent with other geophysical data. The predicted upwelling conduit lies directly beneath the highest elevations (~2 km) in the Great Basin (Fig. 11). In addition, reconciling crustal thicknesses, low gravity, and the high elevation data throughout the Great Basin shows a large buoyancy anomaly in the upper mantle (Parsons et al., 1994). Although these authors suggest that this anomaly is a remnant of the hypothesized Yellowstone plume head that erupted ca. 17 Ma throughout the northern Great Basin, it is also possible that the upwelling predicted by the splitting data alone is providing at least part of this buoyancy anomaly. Furthermore, there is a low-velocity anomaly at ~350 km depth that is elongated in the northeast-southwest orientation (Van der Lee and Nolet, 1997) within the predicted stagnation streamline of the upwelling (the line separating upwelling material from normal asthenosphere), although the resolution of velocity anomalies at that depth is not clear.

If an upwelling does exist beneath eastern Nevada, the lack of a hotspot track there may suggest that the upwelling has a buoyancy that is largely compositional in origin or is not ascending rapidly enough to produce significant decompression melt. Forward modeling of refracted teleseismic shear waves near the 410 km discontinuity (Song et al., 2004) and receiver function images (Gilbert et al., 2003) suggest the existence of a low-velocity zone above 410 km in northern Nevada, Oregon, and southwest Idaho that pinches out beneath eastern Nevada (the region to the south and east of eastern Nevada was not sampled by the refracted waves). This low-velocity zone appears to have a thickness that varies dramatically over short lateral distances, which Song et al. (2004) suggest means that the low-velocity zone is compositional in origin. They speculate that the zone may have developed due to dense melt segregation of an upwelling with a high water content through the 410 km discontinuity. Within the spatial coverage of their study, the most likely place for such an upwelling is in eastern Nevada, where such a low-velocity zone was resolvable, but not detected.

For the Great Basin PAF model, large *dt* are not found above the predicted conduit, whereas splitting with considerable to large *dt* has been observed above the Eifel, Hawaii (Walker et al., 2001), and Yellowstone (G. Waite, 2003, personal commun.) hotspots. If splitting above these latter hotspots is due to anisotropy within a conduit itself associated with a high water fugacity, the lack of splitting indicates either that there is no upwelling beneath eastern Nevada or that upwelling material has a low water fugacity. This latter view may be consistent with the interpretation of Song et al. (2004) that compositional segregation and dehydration are occurring within a narrow depth range

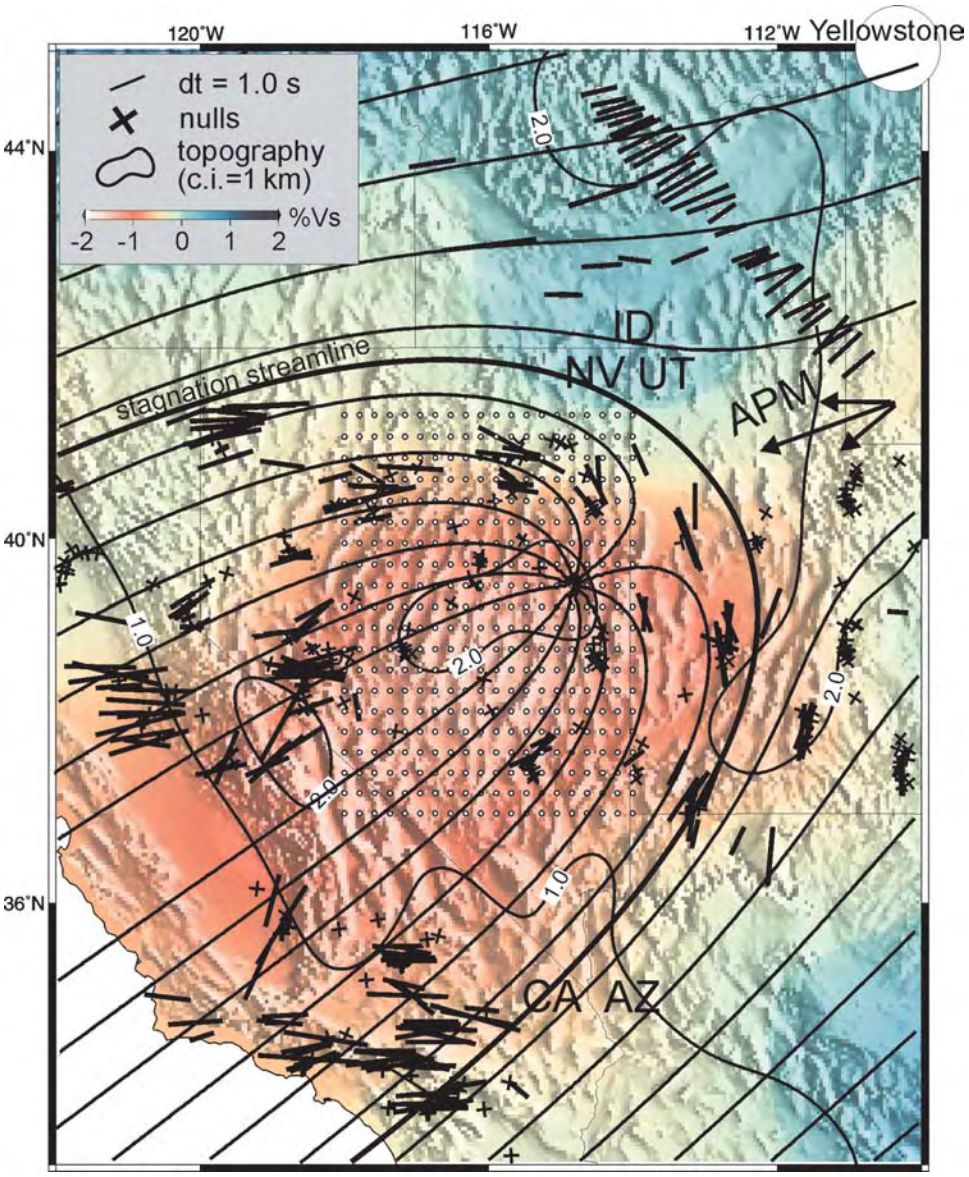

Figure 11. Splitting results in the western United States (ID—Idaho, NV—Nevada, UT—Utah, CA—California, AZ—Arizona). The results across and along the Snake River Plain are station averages from Schutt et al. (1998) and Walker et al. (2004b). All other results are individual splitting measurements plotted above their 200 km piercing-point depth (Savage, 2002). Null measurements—gray crosses oriented so that legs are parallel to the two possible fast directions. Color background—relative S-velocity perturbation at 350 km depth (Van der Lee and Nolet, 1997). APM—absolute plate motion of North America (and 2σ uncertainties), from Gripp and Gordon (2002). White circles—latitude and longitude grid used to find the optimum parabolic asthenospheric flow (PAF) model. Thin black curves—flow lines of the optimum PAF model, which predicts 64% of the variation in fast polarization azimuth and has a stagnation distance of 180 km (Table 1).

above the 410 km discontinuity (the upwelling material in the upper 300 km of the mantle is anhydrous). If the upwelling peridotite is dehydrated, it is also less likely to experience decompression melting and produce a hotspot track.

Hawaii

Walker et al. (2001, 2003) analyzed shear wave splitting recorded on five broadband stations in the central Pacific to determine if and how the anisotropy near Hawaii is significantly different from that at greater distances (Fig. 12). They found a consistency in anisotropy far from the hotspot above oceanic plates of vastly different age. At stations H2O (ca. 50 Ma; see also Vinnik et al., 2003) and JOHN (ca. 110 Ma), ϕ is identical and approximately parallel to Pacific plate motion, with *dt* between 1.1 and 1.4 s.

Close to Hawaii, the story is more complicated. The available data suggest that there may be a two-layer anisotropy model beneath station KIP, where the upper-layer ϕ is parallel to a lattice preferred orientation of olivine fast a-axes induced by shear along the Molokai fracture zone when it was a transform fault (supported by P_n measurements from Raitt et al., 1971; Bibee and Shor, 1976), and the lower-layer ϕ is parallel to the absolute plate motion. Wolfe and Silver (1998) found a similar two-layer

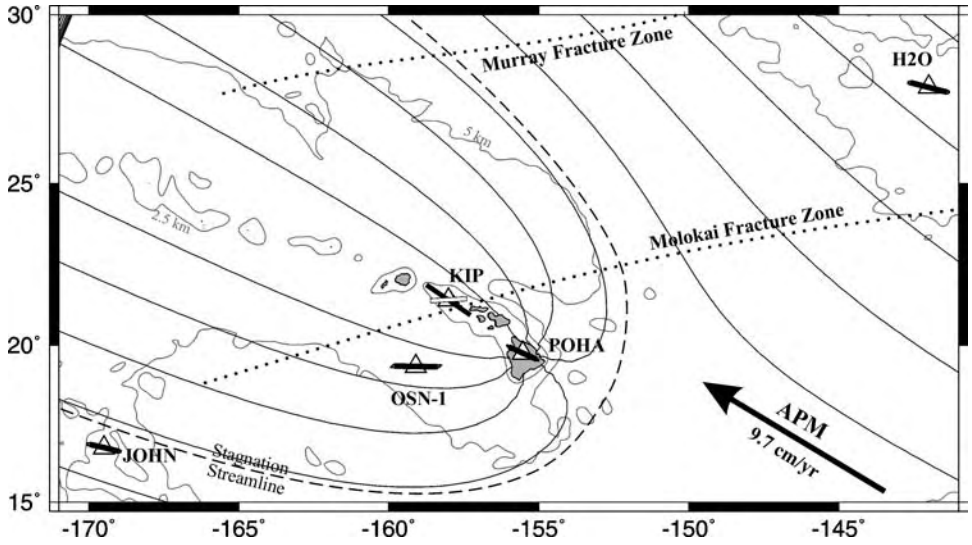

Figure 12. Splitting results around Hawaii and the surrounding region (modified from Walker et al., 2003). Triangles—analyzed stations. Short lines—station splitting estimates. A two-layer model explains splitting at station KIP, with shading reflecting the interpreted depth (white—lithospheric, black—asthenospheric). The parabolic asthenospheric flow model shown explains 75% of the variation in fast polarization azimuth (for the few stations analyzed: OSN-1, POHA, and lower layer beneath KIP) and has a stagnation distance of 300 km.

model for KIP. However, the fact that the apparent *dt* are not fit well by a two-layer model, but seem to be partly a function of back azimuth (not necessarily initial polarization azimuth) hints at a more complicated anisotropy, perhaps a two-layer model with a dipping fast axis in the lower layer. At both KIP and H2O, a single-layer model of orthorhombic olivine with a fast a-axis dipping ~20° toward 280° explains ~50% of the splitting parameter variation (Walker, 2004). A single-layer model with a horizontal fast axis explains the splitting measurements at stations POHA and OSN-1, although these stations recorded far fewer events than were recorded at KIP. Splitting at POHA was also relatively less consistent in that there were many more nulls observed, and a two-layer model similar to that at KIP cannot be ruled out due to a large uncertainty in one of the few non-null measurements.

At OSN-1 ϕ deviates from that at POHA and KIP (lower layer) by ~30°. The 2σ error for OSN-1, KIP, and POHA is about ± 5°, which indicates that this deviation is significant. Whereas Walker et al. (2001) have analyzed three events for OSN-1, Collins et al. (2002) have analyzed six events, and they report a similar average ϕ, which deviates from that at POHA and KIP by ~20°. A similar deviation in the asthenosphere is also observed in global surface wave azimuthal anisotropy data (Montagner and Guillot, 2000), although the lateral resolution is not as good as that provided by splitting. In addition, a regional surface wave anisotropy study across the SWELL pilot array (Laske and Orcutt, 2000), located ~400 km west-southwest of Hawaii, resolves a similar rotation of the northwest-southeast fast S-velocity direction in the lower lithosphere and asthenosphere, although the actual azimuths themselves are not identical to the observed ϕ. A PAF model centered just southeast of station POHA and opening in the direction of absolute plate motion is consistent with this rotation (Fig. 12), and it explains 75% of the ϕ variation from the mean (Table 1). However, this PAF model is not uniquely determined from those few data points.

The stagnation distance r_s = 300 km for the Hawaii PAF model (Fig. 12; Walker et al., 2001). Sleep (1990) estimated this parameter to be 350–450 km based on the topographic area of the swell and assuming an asthenospheric flow speed of half the plate speed. However, the flow speed is more like 60%–70% of the plate speed (Ribe and Christensen, 1994), which revises Sleep's estimate to r_s = 250–375 km and brackets the 300 km estimate in Figure 12. Of course additional splitting data must be collected (especially on the seafloor away from the possible complications associated with the hotspot axis) if one is to determine the optimum parameters of the PAF pattern from the anisotropy data alone.

Iceland

Bjarnason et al. (2002) measured the splitting of core-refracted shear phases (SKS, SKKS, PKS) recorded on the ICEMELT seismic network, which consisted of fifteen temporary broadband stations deployed throughout Iceland in 1993–1995 (Fig. 13). High levels of microseismic noise required harsh frequency filtering prior to making the measurements. However, the measurements were still constrained, and this allowed the authors to determine that there were no significant variations in splitting parameters as a function of back azimuth and initial polarization azimuth. Consequently they used the stacking algorithm of Wolfe and Silver (1998) to calculate the optimum single-layer anisotropy models with horizontal fast axes.

There does not appear to be a PAF pattern in the observed ϕ beneath Iceland. Instead Bjarnason et al. (2002) divided the station splitting estimates based on similarity into two groups separated by the northeast-southwest–trending neovolcanic rift that cuts through the center of Iceland. The eastern group displays stronger anisotropy, with a *dt* of 0.7–1.4 s and a NW-NNW ϕ. Anisotropy is weaker to the west, with delays of 0.2–1.0 s and a broader range of ϕ between north-northwest and northeast.

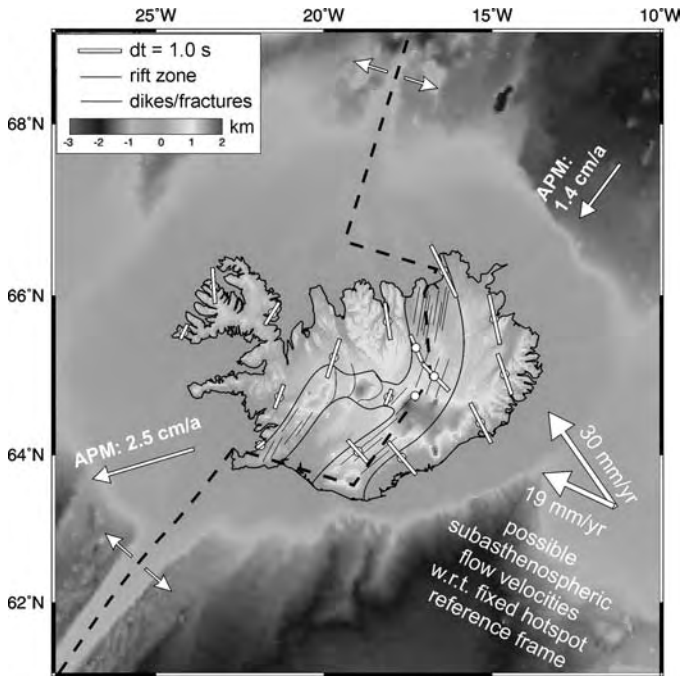

Figure 13. Splitting results around Iceland. White lines—station splitting estimates from Bjarnason et al. (2002). Background color map—topography. White vectors—absolute plate motion (APM) for the North American and Eurasian plates (Gripp and Gordon, 2002). Dashed line—mid-Atlantic spreading ridge, which bisects Iceland through a zone of fissures and dike intrusions. The preferred interpretation of Bjarnason et al. (2002) is that the averages of ϕ in both the western and the eastern half of Iceland are explained by the relative motion between the moving plates and an underlying 30 mm/a mantle flow toward N34°W (Fig. 3). We recalculate a mantle flow velocity of 19 mm/a toward N65°W using the revised Gripp and Gordon (2002) plate motions.

Bjarnason et al. (2002) considered several hypotheses involving mantle flow and aligned magma-filled lenses to explain their data. Their preferred interpretation is that the observed ϕ is parallel to the orientation of the relative motion between the lithosphere and the subasthenosphere relative motion, from which they calculate a common subasthenospheric horizontal velocity of N34°W at 30 mm/a. They state that this model is not inconsistent with an upwelling model beneath Iceland, because a thinning of the transition zone, imaged by receiver function migration (Shen et al., 2002), suggests that the upwelling may be occurring ~100 km to the south of the upwelling that was imaged with body wave tomography (Wolfe et al., 1997). However, the calculation of asthenospheric flow based on splitting is strongly dependent on the plate motion models. For example, using the revised HS3-NUVEL1A absolute plate motion model (Gripp and Gordon, 2002), we calculated a subasthenospheric velocity of 19 mm/a toward N65°W, which is perpendicular to the spreading ridge and subparallel to the fast anisotropy direction predicted by Becker et al. (2003) by modeling the anisotropy expected to develop between the convecting mantle and moving plates in a no-net-rotation reference frame.

If either the north-northwest or west-northwest subasthenospheric flow model is correct, there is an additional anisotropic complexity in the ~75-km-thick Icelandic lithosphere (Bjarnason, 1999) and/or the asthenosphere beneath Iceland that gives rise to the lateral variability in splitting observed in the western group. For example, the variability may be related to different domains of magma-filled lenses or dikes aligned in different orientations (Kendall, 1994); to two-layer anisotropy associated with an olivine lattice preferred orientation in the lithosphere due to ductile stretching (Silver and Savage, 1994), which was not resolvable given the individual splitting measurement errors; or to one of several mechanisms that influence the development of a lattice preferred orientation associated with mantle deformation, such as: (1) the effects of dynamic recrystallization that was recently modeled (Kaminski and Ribe, 2002; Fig. 4); (2) the effects of a more complicated mantle upwelling than that predicted by a simple cylindrical conduit impinging upon a flat lithosphere-asthenosphere boundary (e.g., Ritter et al., 2001); (3) a rheology change during gravitational spreading away from the upwelling, perhaps associated with melt and volatile extraction (e.g., Saltzer and Humphreys, 1997); or (4) the effect of high water content in the upwelling mantle material within the conduit (Jung and Karato, 2001; Karato, 2003). These possible complexities must be considered because of the lack of depth resolution in the splitting data and because the data recorded within the east and west subgroups vary considerably from their respective averages. Additional seismic data collected at many locations on the seafloor around Iceland, away from possible complexities associated with pockets of partial melt, hold great promise for distinguishing with more certainty the source(s) of Icelandic anisotropy.

Afar

Ethiopia is similar to Iceland in some respects, with a bisecting north-south rift, numerous basaltic dikes intruding into the rift zone, and a nearby mantle hotspot (Woodhouse and Dziewonski, 1984; Hadiouche et al., 1989; Ritsema and van Heijst, 2000; Debayle et al., 2001; Fig. 14). The main differences between the two are that Ethiopia is still in the early stages of rift development whereas Iceland sits atop a fully developed spreading center, the spreading rates for the Main Ethiopian Rift are far slower, and Ethiopia is in a region comprised in part of Precambrian continental lithosphere whereas Icelandic lithosphere is being created locally.

Figure 14 shows the single-layer splitting estimates from numerous studies in East Africa and Saudi Arabia. Gashawbeza et al. (2004) have made SKS-splitting measurements on twenty-six broadband stations of the Ethiopian Broadband Seismic Experiment (Nyblade and Langston, 2002). Kendall et al. (2003), Maguire et al. (2003), and Ayele et al. (2004) also made splitting measurements for several stations inside the Main Ethiopian Rift. Barruol and Ismail (2001) analyzed shear wave splitting on station ATD, located near the Afar triple junction. These studies

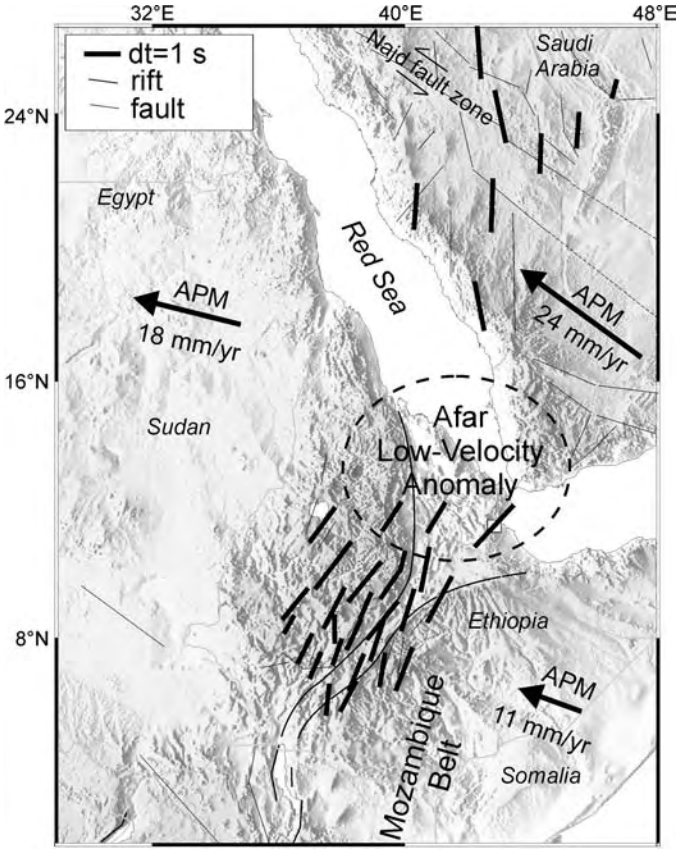

Figure 14. Splitting results for the Afar region. Short lines—station splitting estimates from Wolfe et al. (1999; Saudi Arabia), Barruol and Ismail (2001; Djibouti), and Gashawbeza et al. (2004; Ethiopia). Black vectors—absolute plate motion (APM) in a fixed hotspot reference frame (Gripp and Gordon, 2002; Sella et al., 2002; Fernandes et al., 2004). Thick black curves—Main Ethiopian Rift. Thin black lines—faults that help define the structural elements in the Precambrian basement. The interpretation of Gashawbeza et al. (2004) is that the Ethiopian splitting data characterize the orientation of olivine lattice preferred orientation fossilized in the lithosphere since its creation during past orogenic episodes (Fig. 3). Wolfe et al. (1999) list this as a possible interpretation for splitting in Saudi Arabia, but also note that the data are compatible with a lattice preferred orientation of olivine at the base of the lithosphere due to lateral asthenospheric flow associated with the Afar upwelling. Here the hotspot is indicated by an oval based on surface wave (A. Sebai, 2004, personal commun.) and body wave tomography (Montelli et al., 2004).

found that ϕ is fairly consistent throughout Ethiopia with a NNE-NE orientation, although a significant 15–20° rotation from north-northeast to northeast exists from northwest to east across the network. The *dt* are less consistent and vary between 0.5 and 1.7 s, with an increasing trend within the rift toward the Afar triple junction. In Saudi Arabia Wolfe et al. (1999) made SKS-splitting measurements on eight temporary broadband stations, and they found generally north-south ϕ, but *dt* that varies from 0.5 to 1.5 s.

In Ethiopia Gashawbeza et al. (2004) interpreted a correlation between ϕ and the trends of the Paleozoic suture zones reconstructed by Berhe (1990) as due to a lattice preferred orientation of olivine inherited and preserved from Paleozoic orogenic events. Although the geological structural trends at the surface, in the few places they are exposed, are oriented NNW-NNE (C. Ebinger, 2004, personal commun.), the splitting results could be reflecting the dominant lattice preferred orientation in the lithosphere that is obscured by surficial geology or that characterizes most of the lithosphere beginning at a depth of a few kilometers. This hypothesis has also been proposed to explain, at least in part, the splitting in Saudi Arabia (Wolfe et al., 1999), Tanzania and Kenya (Barruol and Ismail, 2001; Walker et al., 2004a), and South Africa (Silver et al., 2001; Fouch et al., 2004).

The general uniformity and orientation of ϕ throughout Ethiopia make it compatible to a certain extent with several possible anisotropy models. Although there is no noticeable change in *dt* between rift and off-rift stations, the *dt* in the rift are probably too large to be explained by fossilized anisotropy in the presumably thinned lithosphere because orogenic events would most likely give rise to a maximum S anisotropy of ~4% (Mainprice and Silver, 1993). Consequently, Gashawbeza et al. (2004) interpret the splitting in the rift as due to a combination of fossilized anisotropy in the lithosphere and magma-filled lenses in the lithosphere and the asthenosphere aligned by a WNW-ESE least compressive stress orientation (σ_3; Vauchez et al., 2000). Kendall et al. (2003) and Ayele et al. (2004) interpret their splitting measurements as due to aligned magma-filled lenses, which is supported by a significant increase in *dt* toward the Afar triple junction assuming that the porosity of melt increases toward it. However, the crustal maximum horizontal compressive stress orientation indicators in the Afar can be divided into two groups: NNW-SSE and WNW-ESE (Sperner et al., 2003). If the maximum stress orientations in the upper crust predict those at greater depths, neither of the two groups of stress indicators predicts the observed NNE-NE ϕ.

The width of the Afar hotspot (Fig. 14) is defined by the approximate low (–4%) S-velocity anomaly contour between 50 and 300 km depth (A. Sebai, 2004, personal commun.) and the approximate location from recent global body wave tomography at the transition zone (Montelli et al., 2004). If this hotspot is associated with an upwelling, for pure radial flow Gashawbeza et al. (2004) point out that there is a significant deviation between predicted and observed ϕ at the Ethiopian stations farthest to the northwest and at the easternmost stations. Furthermore, there is no PAF ϕ pattern as one might expect for an upwelling, slowly moving plate, and flat lithosphere-asthenosphere boundary. However, because ~90% of ϕ are consistent with radial flow, these authors note that a modification of flow by other factors (such as a nontypical conduit shape, the channelization of asthenospheric flow by topography along the lithosphere-asthenosphere boundary, or the creation of space via rifting) could explain all ϕ. In this view the upwelling material is moving toward the southwest beneath Ethiopia and toward the north beneath Saudi Arabia, inducing shear and olivine lattice preferred

orientation anisotropy along the base of both plates, which was one of the hypotheses proposed by Wolfe et al. (1999) to explain splitting beneath Saudi Arabia. Because one would expect the lateral velocity of the upwelling material to increase toward the upwelling center, this model also predicts the observed increase in *dt* toward the Afar triple junction.

We can estimate the speed required of the lateral asthenospheric flow to produce the observed ϕ variation across the Main Ethiopian Rift by performing the same calculation as for Iceland (Bjarnason et al., 2002). The geologic rate of spreading across the rift is slow, with a maximum estimate of ~7 mm/a (Sella et al., 2002; Fernandes et al., 2004), giving the Somalia microplate a maximum absolute plate motion velocity of 11 mm/a toward 290°. To explain the 18° of ϕ rotation we calculate a subasthenospheric flow direction of N6°W at 20 mm/a. However, this velocity is poorly constrained due to the small ϕ and plate motion deviations. In fact, if the rate of spreading is assumed to be insignificant compared with the 18 mm/a absolute plate motion of Nubia (Africa), the direction of subasthenospheric flow velocity can be anywhere from 225° clockwise to 025°. For upwelling material to be flowing laterally from the upwelling toward 225° beneath the array, the flow speed must be at least 50–100 mm/a beneath the seismic network. To explain the north-south ϕ in Saudi Arabia (Wolfe et al., 1999), a similar calculation yields a minimum subasthenospheric flow velocity of ~150–200 mm/a for the HS3-NUVEL1A Arabia absolute plate motion (Gripp and Gordon, 2002). Although some plates move at comparable speeds (e.g., Pacific at 103 mm/a), these values are probably too high to be realistic beneath Ethiopia and Saudi Arabia, especially considering that the observed north-south ϕ beneath Saudi Arabia exist much farther from the upwelling than the Ethiopian stations.

Thus ϕ beneath Ethiopia and the Afar can be reasonably explained entirely by lateral flow originating at an Afar upwelling only if (1) the absolute plate motion of the Africa plate is slower than that given by the HS3-NUVEL1A model (Gripp and Gordon, 2002); (2) lithospheric thickening toward Sudan, which would be expected if the mantle lithosphere has stretched during the last 30 m.y. over a broader region rather than directly beneath the rift, encourages radial flow from the upwelling to bend toward the southwest beneath Ethiopia and to the northwest beneath the Red Sea (Bormann et al., 1996; Ebinger and Sleep, 1998); and (3) the speed of background mantle flow associated with global convection cells (e.g., Becker et al., 2003) is not as significant as that due to an Afar upwelling.

In summary, it seems that the existing splitting observations in the Afar are simple, but what they say about the anisotropy beneath the surface is not. Because of the distinct possibility that several anisotropy sources have influenced the splitting, in terms of testing the plume hypothesis it can only be said that the existing splitting data are not inconsistent with a plumelike upwelling. It seems likely that this ambiguity will be resolved when we have better constraints on the depth distribution of anisotropy as well as higher-resolution tomographic images beneath the Afar region.

FORTHCOMING DATA

Several other hotspots are the focus of current seismic investigation. These include the Yellowstone (R. Smith, 2004, personal commun.), Society Islands (G. Barruol, 2004, personal commun.), and Galapagos (D. Toomey, 2004, personal commun.) hotspots. In addition, a large volume of seismic data will be collected on the seafloor around Hawaii during 2005–2006 (G. Laske and C. Wolfe, 2004, personal commun.) and possibly in the future around Iceland (N. Ribe, 2003, personal commun.).

DISCUSSION

The results reported earlier show that shear wave splitting can help improve our understanding of the interaction between the lithosphere and the asthenosphere around some hotspots. Specifically, simple PAF explains 61% and 64% of the variation of the fast polarization azimuths for the Eifel and the Great Basin, respectively (Table 1). These two PAF models are uniquely determined from the splitting data alone, the model parameters have small error bars, and the model parameters as well as the models themselves are consistent with other geophysical data. In these two regions, all these data suggest that a plumelike upwelling exists. However, these regions lack certain observations that support the classic plume model, such as a recognizable hotspot track associated with both upwellings and flood basalts associated with the Eifel upwelling. Although it seems natural to link the PAF model to an active upwelling, without guidance from quantitative flow and lattice preferred orientation modeling, the lack of a hotspot track might mean that the upwellings are passive in nature, a result of return flow from subduction or the filling of space created by lithosphere stretching. Of course, the data are not inconsistent with a mantle plume either, because factors such as composition and water fugacity play an important role in the buoyancy and solidus temperature of upwelling material. In particular, a dry, compositionally buoyant plume is less likely to produce volcanism than a wet, thermally buoyant plume.

For the Hawaii hotspot, there are too few stations to uniquely determine the origin of splitting, as well as find a unique PAF model that fits the data. However, the PAF model shown, which is consistent with results from finite-difference modeling of Ribe and Christensen (1994, 1999), explains 75% of the variation in the splitting data, indicating that the few measurements are consistent with a plumelike upwelling model for Hawaii.

The PAF model parameters can put constraints on upwelling dynamics. For example, the stagnation distance is defined as the distance upwind from the vertical conduit to the point where the radial spreading velocity equals that of the background asthenospheric flow (Sleep, 1990). For the simple PAF pattern this distance is $r_s = u/sh$, where u is the upwelling volumetric flow rate, s is the background asthenospheric flow speed (assumed to be 60%–70% of the plate speed; Ribe and Christensen, 1994), and h is the thickness of the mechanical asthenosphere (the zone into which the spreading plume material flows). The buoyancy

TABLE 1. PARABOLIC ASTHENOSPHERIC FLOW PATTERN PARAMETERS AND CORRELATION TO A MODEL OF A PLUMELIKE UPWELLING BENEATH A MOVING PLATE IN A FIXED HOTSPOT REFERENCE FRAME

	R^2	Center latitude	Center longitude	Parabolic width (km)	Pattern opening direction	Absolute plate motion
Eifel	0.61	50.31 ± 0.17°	7.05 ± 0.45°	60 ± 15	260 ± 20°	239 ± 44°
Nevada	0.64	39.49 ± 0.11°	–114.84 ± 0.11°	180 ± 25	240 ± 5°	252 ± 19°
Hawaii	0.75	19.64°	–155.30°	300	295°	300 ± 9°

Note: Uncertainty values indicate the 95% confidence limits. R^2 is the variation of ϕ from the mean explained by the model (maximum of 1.0). The results for Eifel and Nevada are derived from a grid search, whereas that for Hawaii is from a forward model based loosely on a priori constraints.

flux is defined as the rate at which the upwelling supplies a buoyancy anomaly beneath the lithosphere, and has traditionally been ascribed to thermal buoyancy $B = \rho_m \alpha \Delta T u$, where ρ_m is the normal asthenosphere density, a is the thermal expansion coefficient (3.5×10^{-5} K^{-1}), and ΔT is the excess plume temperature (Sleep, 1990). However, compositional buoyancy could also contribute to the total buoyancy flux both beneath the swell and in the conduit itself (e.g., Saltzer and Humphreys, 1997; Ribe and Christensen, 1999). Using r_s = 300 km (Fig. 12), the B of 2200–3500 kg/s and ΔT = 300 K for Hawaii (Ribe and Christensen, 1999), and the absolute plate motion of 100 mm/a (Gripp and Gordon, 2002), we calculate h = 100–180 km, which may be considered an upper bound on the vertical thickness of the upwelling material that is the least viscous and most rapidly spreading beneath the plate. This thickness estimate is consistent with that inferred by Gaboret et al. (2003), who used global seismic velocity tomographic images and a velocity-to-density relationship from Karato (1993) to find a sublithospheric low-viscosity channel (10^{19}–10^{20} Pa s) at 100–300 km depth beneath the Pacific basin. Using our value of h and the parameters stated earlier, we note that the upwelling volumetric flow rate $u = 2\pi r_s s h$ and calculate u = 340–740 m^3/s for Hawaii, which is larger than the ~300 m^3/s calculated by Sleep (1990). Using the same thickness h for beneath the Great Basin and the west central Eurasian plate (a questionable assumption used here for heuristic purposes only), we calculate u = 50–140 m^3/s and 10–40 m^3/s for the Great Basin and Eifel upwellings, respectively. Although one could go further and use these upwelling rates and tomographic estimates of upper-mantle velocity to calculate buoyancy fluxes, the recent evidence for compositional buoyancy associated with residual material depleted of denser components during the process of melt segregation makes such an approach questionable (e.g., Saltzer and Humphreys, 1997; Ribe and Christensen, 1999). As mentioned earlier, the lack of a hotspot track beneath eastern Nevada may suggest that a large portion of the ~100 m^3/s volumetric flow there is due to a passive upwelling or to the upwelling of compositionally buoyant, dehydrated mantle (Walker et al., 2004b).

Wolfe and Solomon (1998) calibrated the potential effects of magma-filled lenses on teleseismic splitting by measuring splitting across the rapidly spreading southern East Pacific Rise, an extending region thought to have a significant magma supply without the complications of fossilized lithospheric anisotropy. They found ϕ parallel to the direction of absolute plate motion, with *dt* between 0.8 and 2.2 s, i.e., the opposite direction for evidence of anisotropy due to vertical magma-filled lenses (which are simply predicted to be parallel to the East Pacific Rise). Rather their data suggest that relative motion between the spreading plates and the underlying mantle is the dominant source of anisotropy.

The Afar and Iceland hotspots are associated with relatively slow and fast spreading ridges, respectively. Iceland is associated with relatively vigorous volcanism, whereas the Afar is not. Furthermore, the Ethiopian seismic array was located at a distance of 50–500 km from the Afar hotspot in a region of Proterozoic terranes that have experienced several tectonic episodes, which might have led to fossilized lithospheric anisotropy (Fig. 14). The Iceland array was located directly above the hotspot on new oceanic lithosphere (Fig. 13). In view of these differences, it is not surprising that the characteristics of observed splitting are also different. Splitting is generally coherent across Ethiopia and across Saudi Arabia, but varies remarkably in Iceland. A parabolic pattern in ϕ is not observed around Iceland or, thus far, in the Afar region. The existence of splitting, though, which obviously indicates anisotropy from at least one source beneath these regions, is not inconsistent with a plumelike upwelling because an asthenospheric signal could be masked by another source of anisotropy.

Based on the results of Wolfe and Solomon (1998), one might expect that anisotropy would not be due to aligned magma-filled lenses in regions of less vigorous volcanism such as the Main Ethiopian Rift. Any existing fossilized lithospheric anisotropy beneath this rift from past orogenic events has probably been modified, if not erased in part, due to dynamic recrystallization and melt intrusion. These other data may therefore suggest that the general uniformity in *dt* observed on rift and off-rift stations in Ethiopia by Gashawbeza et al. (2004) is not a perfect balance between fossilized anisotropy off the axis and magma-filled lenses beneath it. Rather it may be equally plausible that the difference in relative motion between the plates and laterally spreading Afar upwelling is the dominant source of anisotropy beneath Ethiopia and Saudi Arabia. In this view, the observed splitting can be used to map the direction and speed of mantle flow beneath the lithosphere (e.g., Silver and Holt, 2002), which can help define the geometry of the likely nonflat lithosphere-asthenosphere boundary. Of course fossilized lithospheric aniso-

tropy may still be the cause of splitting off the rift axis in Ethiopia, which predicts a mantle lithospheric thickness of 55–190 km (Mainprice and Silver, 1993).

The lithosphere and the asthenosphere beneath Iceland (Bjarnason et al., 2002) likely have a higher melt porosity than beneath Ethiopia and the East Pacific Rise, and therefore the variations in splitting observed there may be a result of aligned magma-filled lenses. Nonetheless, the existence of splitting beneath Iceland, as beneath the Afar, prohibits one from ruling out plate/upwelling relative motion as an important contributor to splitting. Such an upwelling may explain the average splitting ϕ observed in the eastern and western sides of Iceland using the estimate of Bjarnason et al. (2002) for the subasthenospheric flow velocity of 30 mm/a at N34°W. Using the revised Eurasian and North American plate motion estimates of Gripp and Gordon (2002), we calculate a revised subasthenospheric flow rate of 19 mm/a toward N65°W.

FUTURE WORK

There is much work that remains to be done around hotspots to better refine our knowledge about the relationships between anisotropy, mantle flow, deformation mechanisms, melt segregation/migration, and water content. In places where numerous high-quality splitting measurements vary systematically as a function of back azimuth, initial polarization azimuth, or incidence angle, one can use a variety of existing techniques to characterize multiple-layer anisotropy (e.g., Silver and Savage, 1994; Montagner et al., 2000). In regions where existing splitting measurements vary appreciably laterally, these relationships can be investigated using currently available techniques such as waveform modeling to forward-model the observed lateral variation in splitting (e.g., Tommasi, 1998; Rümpker et al., 1999, 2003). Around hotspots where splitting measurements do not vary appreciably laterally (e.g., Ethiopia), existing surface wave tomography techniques should be very helpful in determining the depth of azimuthal anisotropy and the source of splitting (e.g., Freybourger et al., 2001; Weeraratne et al., 2003), possibly allowing one to rule out a number of otherwise permissible models that explain the splitting alone. To this end, it is also important to point out that if a surface wave inversion for anisotropy, using a large dataset from a good distribution of back azimuths, detects only radial $V_{SH} > V_{SV}$ anisotropy within the depth of resolution, shear wave splitting recorded in the same region reflects only (1) anisotropy where the fast a- and intermediate c-axes are in the horizontal plane and the slow b-axes are vertical or (2) anisotropy from greater depths. Additional techniques should also be explored to measure anisotropy as a function of 3D space with resolutions that are higher than that currently provided by surface wave anisotropy tomography.

Although considerable advances have been made, there are still many tectonic and geodynamic models that remain to be critically tested. The plume hypothesis is an excellent example. To help resolve this debate a self-consistent approach to future plume hypothesis testing is required. Using observations of seismic anisotropy, we propose the following generalized approach, part of which has been implemented by the works of Becker et al. (2003) and Gaboret et al. (2003) on global anisotropy. Shear wave splitting data recorded around hotspots should be used to correct S phases that are used in S-velocity and Q tomographic imaging, which will reduce the mislocation of back-projected energy and reduce vertical smearing. P-velocity tomographic imaging should also be performed. The resulting 3D velocity images can then be patched into global 3D images; mapped to temperature, buoyancy, and perhaps other rheological parameters; and accepted as input into geodynamic models. These models can then be back-projected in time for several m.y., then run forward to predict the mantle flow, interactions with moving plates, olivine lattice preferred orientation, melt segregation associated with the hotspot or upwelling, and a variety of other hypothesized phenomena that give rise to anisotropy. Observations of seismic anisotropy can then be forward-modeled from these geodynamic models using a range of techniques (ray-based to full wavefield modeling). The recent advances in computational power can be used in multidimensional grid searches to find the optimum tectonic/geodynamic model that simultaneously explains a variety of seismic anisotropy datasets, thereby giving one a self-consistent process by which to test a full range of hypotheses that explain mantle hotspots, even in regions where the anisotropic signal due to active mantle flow is obscured by unrelated lithospheric anisotropy.

ACKNOWLEDGMENTS

Our work was funded in part by National Science Foundation Grant EAR-0107080. We thank the Eifel Plume Team and the many institutions who helped acquire the Eifel Network seismological data. Permanent-station data were provided by the ORFEUS (Observatories and Research Facilities for European Seismology), IRIS (Incorporated Research Institutions for Seismology), and GEOFON (Geo-Forschungs-Netz) data centers. We thank the following people for fruitful discussions and for sharing their data or programs: T. Becker, U. Christensen, R. Gordon, G. Helffrich, B. Holtzman, M. Jordan, S.-I. Karato, R. Montelli, N. Ribe, J. Ritter, G. Rümpker, M. Savage, H. Schmeling, D. Schutt, A. Sebai, and P. Silver. SAC2000 (Seismic Analysis Tools) and GMT (Generic Mapping Tools) were used to generate figures. We thank T. Becker, G. Foulger, D. Forsythe, and J.-P. Montagner for helpful comments in reviewing this manuscript.

REFERENCES CITED

Allegre, C.J., 2002, The evolution of mantle mixing: Philosophical Transactions of the Royal Society of London, v. 360, p. 1–21.

Alsina, D., and Snieder, R., 1995, Small-scale sublithospheric continental mantle deformation: Constraints from SKS splitting observations: Geophysical Journal International, v. 123, p. 431–448.

Anderson, D.L., 1994, The sublithospheric mantle as the source of continental

flood basalts: The case against the continental lithosphere and plume head reservoirs: Earth and Planetary Science Letters, v. 123, p. 269–280, doi: 10.1016/0012-821X(94)90273-9.

Anderson, D.L., 2000, The edges of the mantle, *in* Gurnis, M., et al., eds., The core-mantle boundary region: Washington, D.C., American Geophysical Union, p. 255–271.

Ayele, A., Stuart, G., and Kendall, J.-M., 2004, Insights into rifting from shear wave splitting and receiver functions: An example from Ethiopia: Geophysical Journal International, v. 157, p. 354–362, doi: 10.1111/j.1365-246X.2004.02206.x.

Babuska, V., and Plomerová, J., 1993, Lithospheric thickness and velocity anisotropy—Seismological and geothermal aspects: Tectonophysics, v. 225, p. 79–89, doi: 10.1016/0040-1951(93)90250-N.

Barruol, G., and Ismail, W.B., 2001, Upper mantle anisotropy beneath the African IRIS and Geoscope stations: Geophysical Journal International, v. 146, p. 549–561, doi: 10.1046/j.0956-540x.2001.01481.x.

Becker, T.W., Kellogg, J.B., Ekström, G., and O'Connell, R.J., 2003, Comparison of azimuthal seismic anisotropy from surface waves and finite strain from global mantle-circulation models: Geophysical Journal International, v. 155, p. 696–714, doi: 10.1046/j.1365-246X.2003.02085.x.

Berhe, S.M., 1990, Ophiolites in northeast and east Africa: Implications for Proterozoic crustal growth: Journal of the Geological Society of London, v. 147, p. 41–57.

Bibee, L.D., and Shor, G.G., 1976, Compressional wave anisotropy in the crust and upper mantle: Geophysical Research Letters, v. 3, p. 639–642.

Bijwaard, H., and Spakman, W., 1999, Tomographic evidence for a narrow whole mantle plume below Iceland: Earth and Planetary Science Letters, v. 166, p. 121–126, doi: 10.1016/S0012-821X(99)00004-7.

Bijwaard, H., Spakman, W., and Engdahl, E.R., 1998, Closing the gap between regional and global travel time tomography: Journal of Geophysical Research, v. 103, p. 30,055–30,078, doi: 10.1029/98JB02467.

Bjarnason, I.T., 1999, How thick is the lithosphere in Iceland? How large is the velocity inversion in the asthensophere and what does it mean?: Eos (Transactions, American Geophysical Union), v. 80, p. F645.

Bjarnason, I.T., Silver, P.G., Rümpker, G., and Solomon, S.C., 2002, Shear wave splitting across the Iceland hot spot: Results from the ICEMELT experiment: Journal of Geophysical Research, v. 107, no. B12, 2382, doi: 10.1029/2001JB000916.

Bormann, P., Burghardt, P.-T., Makeyeva, L.I., and Vinnik, L.P., 1993, Teleseismic shear-wave splitting and deformations in Central Europe: Physics of the Earth and Planetary Interiors, v. 78, p. 157–166, doi: 10.1016/0031-9201(93)90153-Z.

Bormann, P., Grunthal, G., Kind, R., and Montag, H., 1996, Upper mantle anisotropy beneath Central Europe from SKS wave splitting: Effects of absolute plate motion and lithosphere-asthenosphere boundary topography?: Journal of Geodynamics, v. 22, p. 11–32, doi: 10.1016/0264-3707(96)00014-2.

Collins, J.A., Vernon, F.L., Orcutt, J.A., and Stephen, R.A., 2002, Upper mantle structure beneath the Hawaiian swell: Constraints from the ocean seismic network pilot experiment: Geophysical Research Letters, v. 29, 1522, doi:10.1029/ 2001GL013302.

Courtillot, V., Davaille, A., Besse, J., and Stock, J., 2003, Three distinct types of hotspots in the Earth's mantle: Earth and Planetary Science Letters, v. 205, p. 295–308, doi: 10.1016/S0012-821X(02)01048-8.

Crampin, S., 1991, Wave propagation through fluid-filled inclusions of various shapes: Interpretation of extensive-dilatancy anisotropy: Geophysical Journal International, v. 104, p. 611–623.

Davies, G.F., and Richards, M.A., 1992, Mantle convection: Journal of Geology, v. 100, p. 151–206.

Debayle, E., Lévêque, J.J., and Cara, M., 2001, Seismic evidence for a deeply rooted low velocity anomaly in the upper mantle beneath the northeastern Afro/Arabian continent: Earth and Planetary Science Letters, v. 193, p. 423–436, doi: 10.1016/S0012-821X(01)00509-X.

Dietz, R.S., 1961, Continent and ocean basin evolution by spreading of the sea floor: Nature, v. 190, p. 854–857.

Ebinger, C., and Sleep, N.H., 1998, Cenozoic magmatism in central and east Africa resulting from impact of one large plume: Nature, v. 395, p. 788–791, doi: 10.1038/27417.

Edel, J.B., and Fluck, P., 1989, The upper Rhenish shield basement: Tectonophysics, v. 169, p. 303–316, doi: 10.1016/0040-1951(89)90093-0.

Fernandes, R.M.S., Ambrosius, B.A.C., Noomen, R., Bastos, L., Combrinck, C.L., Miranda, J.M., and Spakman, W., 2004, Angular velocities of Nubia and Somalia from continuous GPS data: Implications on present-day relative kinematics: Earth and Planetary Science Letters, v. 222, p. 197–208, doi: 10.1016/j.epsl.2004.02.008.

Fischer, K.M., and Wiens, D.A., 1996, The depth distribution of mantle anisotropy beneath the Tonga subduction zone: Earth and Planetary Science Letters, v. 142, p. 253–260, doi: 10.1016/0012-821X(96)00084-2.

Fouch, M.J., Silver, P.G., Bell, D.R., and Lee, J.N., 2004, Small-scale variations in seismic anisotropy near Kimberley, South Africa: Geophysical Journal International, v. 157, p. 764–774, doi: 10.1111/j.1365–246X.2004.02234.x.

Foulger, G.R., Pritchard, M.J., Julian, B.R., Evans, J.R., Allen, R.M., Nolet, G., Morgan, W.J., Bergsson, B.H., Erlendsson, P., Jakobsdottir, S., Ragnarsson, S., Stefansson, R., and Vogfjord, K., 2001, Seismic tomography shows that upwelling beneath Iceland is confined to the upper mantle: Geophysical Journal International, v. 146, p. 504–530, doi: 10.1046/j.0956-540x.2001.01470.x.

Freybourger, M., Gaherty, J.B., and Jordan, T.H., 2001, Structure of the Kaapvaal craton from surface waves: Geophysical Research Letters, v. 28, p. 2489–2492, doi: 10.1029/2000GL012436.

Gaboret, C., Forte, A.M., and Montagner, J.-P., 2003, The unique dynamics of the Pacific Hemisphere mantle and its signature on seismic anisotropy: Earth and Planetary Science Letters, v. 208, p. 219–233, doi: 10.1016/S0012-821X(03)00037-2.

Gao, S., Davis, P.M., Liu, H., Slack, P.D., Rigor, A.W., Zorin, Y.A., Mordvinova, V.V., Kozhevnikov, V.M., and Logatchev, N.A., 1997, SKS splitting beneath continental rift zones: Journal of Geophysical Research, v. 102, p. 22,781–22,797, doi: 10.1029/97JB01858.

Gashawbeza, E., Klemperer, S., Nyblade, A., Walker, K., and Keranen, K., 2004, Shear-wave splitting in Ethiopia: Precambrian mantle anisotropy locally modified by Neogene rifting: Geophysical Research Letters, v. 31, L18602, doi: 10.1029/2004GL020471.

Gilbert, H.J., Sheehan, A.F., Dueker, K.G., and Molnar, P., 2003, Receiver functions in the western United States, with implications for upper mantle structure and dynamics: Journal of Geophysical Research, v. 108, B5, doi: 10.1029/2001JB001194.

Goes, S., Spakman, W., and Bijwaard, H., 1999, A lower mantle source for central European volcanism: Science, v. 286, p. 1928–1931, doi: 10.1126/science.286.5446.1928.

Gripp, A.E., and Gordon, R.G., 2002, Young tracks of hotspots and current plate velocities: Geophysical Journal International, v. 150, p. 321–361, doi: 10.1046/j.1365-246X.2002.01627.x.

Grunewald, S., Weber, M., and Kind, R., 2001, The upper mantle under Central Europe: Indications for the Eifel plume: Geophysical Journal International, v. 147, p. 590–601, doi: 10.1046/j.1365-246x.2001.01553.x.

Hadiouche, O., Jobert, N., and Montagner, J.-P., 1989, Anisotropy of the African continent inferred from surface waves: Physics of the Earth and Planetary Interiors, v. 58, p. 61–81, doi: 10.1016/0031-9201(89)90096-4.

Hess, H., 1962, The history of ocean basins, *in* Engel, A.E.J., et al., eds., Petrologic studies: A volume to honor A.F. Buddington: Boulder, Colorado, Geological Society of America, p. 599–620.

Illies, J.H., Prodehl, C., Schmincke, H.-U., and Semmel, A., 1979, The Quaternary uplift of the Rhenish shield in Germany: Tectonophysics, v. 61, p. 197–225, doi: 10.1016/0040-1951(79)90298-1.

Jung, H., and Karato, S.-I., 2001, Water-induced fabric transitions in olivine: Science, v. 293, p. 1460–1463, doi: 10.1126/science.1062235.

Jung, S., and Hoernes, S., 2000, The major- and trace element and isotope (Sr, Nd, O) geochemistry of Cenozoic alkaline rift-type volcanic rocks from the Rhön area (central Germany): Petrology, mantle source characteristics and implications for asthenosphere-lithosphere interactions: Journal of Vol-

canology and Geothermal Research, v. 99, p. 27–53, doi: 10.1016/S0377-0273(00)00156-6.

Kaminski, E., and Ribe, E., 2002, Timescales for the evolution of seismic anisotropy in mantle flow: G^3, v. 3, doi: 10.1029/2001GC000222.

Karato, S., 1993, Importance of anelasticity in the interpretation of seismic tomography: Geophysical Research Letters, v. 20, p. 1623–1626.

Karato, S.-I., 2003, Mapping water content in the upper mantle, *in* Eiler, J., ed., Inside the subduction factory: Washington, D.C., American Geophysical Union Monograph 138.

Karato, S.-I., and Wu, P., 1993, Rheology of the upper mantle: A synthesis: Science, v. 260, p. 771–777.

Kendall, J.-M., 1994, Teleseismic arrivals at a mid-ocean ridge: Effects of mantle melt and anisotropy: Geophysical Research Letters, v. 21, p. 301–304, doi: 10.1029/93GL02791.

Kendall, J.-M., Stuart, G., Bastow, I., and Ebinger, C., 2003, Melt migration and mantle anisotropy beneath the Ethiopian rift: Eos (Transactions, American Geophysical Union), v. 84, p. F1125.

Keyser, M., Ritter, J.R.R., and Jordan, M., 2002, 3D shear-wave velocity structure of the Eifel plume, Germany: Earth and Planetary Science Letters, v. 203, p. 59–82, doi: 10.1016/S0012-821X(02)00861-0.

King, S.D., and Anderson, D.L., 1998, Edge-driven convection: Earth and Planetary Science Letters, v. 160, p. 289–296, doi: 10.1016/S0012-821X(98)00089-2.

Laske, G., and Orcutt, J., 2000, The Hawaiian SWELL Experiment: An example for the need of broad-band ocean bottom seismograms: Eos (Transactions, American Geophysical Union), v. 81, p. F819.

Leibecker, J., Gatzemeier, A., Honig, M., Kuras, O., and Soyer, W., 2002, Evidence of electrical anisotropic structures in the lower crust and upper mantle beneath the Rhenish Shield: Earth and Planetary Science Letters, v. 202, p. 289–302, doi: 10.1016/S0012-821X(02)00783-5.

Li, X., Kind, R., Yuan, X., Sobolev, S.V., Hanka, W., Ramesh, D.S., Gu, Y., and Dziewonski, A.M., 2003, Seismic observation of narrow plumes in the oceanic upper mantle: Geophysical Research Letters, v. 30, p. 1334, doi: 10.1029/2002GL015411.

Maguire, P.K.H., Ebinger, C.J., Stuart, G.W., Mackenzie, G.D., Whaler, K.A., Kendall, J.-M., Khan, M.A., Fowler, C.M.R., Klemperer, S.L., Keller, G.R., Furman, T., Mickus, K., Asfaw, L., Ayele, A., and Abebe, B., 2003, Geophysical project in Ethiopia studies continental breakup: Eos (Transactions, American Geophysical Union), v. 84, p. 337, 342–343.

Mainprice, D., and Silver, P.G., 1993, Constraints on the interpretation of teleseismic SKS observations from kimberlite nodules from the subcontinental mantle: Physics of the Earth and Planetary Interiors, v. 78, p. 257–280, doi: 10.1016/0031-9201(93)90160-B.

Meyer, R., 2001, Teleseismische P-Wellendämpfung in der Eifel: Analyse und Tomographie [Ph.D. thesis]: Göttingen, Germany, University of Göttingen.

Milne-Thomson, L.M., 1968, Theoretical hydrodynamics (5th edition): New York, Macmillan.

Montagner, J.-P., 1994, Can seismology tell us anything about convection in the mantle?: Reviews of Geophysics, v. 32, p. 115–137, doi: 10.1029/94RG00099.

Montagner, J.-P., and Guillot, L., 2000, Seismic anisotropy in the Earth's mantle, *in* Boschi, E., et al., eds., Problems in geophysics for the next millennium: Bologna, Italy, Editrice Compositori, p. 217–253.

Montagner, J.-P., Griot-Pommera, D.A., and Lave, J., 2000, How to relate body wave and surface wave anisotropy?: Journal of Geophysical Research, v. 105, p. 19,015–19,027, doi: 10.1029/2000JB900015.

Montelli, R., Nolet, G., Dahlen, F.A., Masters, G., Engdah, E.R., and Hung, S.H., 2004, Finite-frequency tomography reveals a variety of plumes in the mantle: Science, v. 303, p. 338–343, doi: 10.1126/science.1092485.

Morgan, W.J., 1971, Convection plumes in the lower mantle: Nature, v. 230, p. 42–43.

Morgan, W.J., 1972, Plate motions and deep convection: Geological Society of America, v. 132, p. 7–22.

Mueller, B., Wehrle, V., and Fuchs, K., 1997, The 1997 release of the world stress map: http://www.world-stress-map.org/.

Nicolas, A., and Christensen, N.I., 1987, Formation of anisotropy in upper mantle peridotites—A review, *in* Fuchs, K., and Froidevaux, C., eds., Composition, structure, and dynamics of the lithosphere-asthenosphere system, Washington, D.C., American Geophysical Union, Geodynamics Series 16: p. 111–123.

Nyblade, A.A., and Langston, C.A., 2002, Broadband seismic experiments probe the East African rift: Eos (Transactions, American Geophysical Union), v. 83, p. 405–408.

Olson, P., 1990, Hot spots, swells and mantle plumes, *in* Ryan, M.P., ed., Magma transport and storage: New York, John Wiley, p. 33–51.

Parsons, T., Thompson, G., and Sleep, N., 1994, Mantle plume influence on the Neogene uplift and extension of the U.S. western Cordillera?: Geology, v. 22, p. 83–86, doi: 10.1130/0091-7613(1994)022<0083:MPIOTN>2.3.CO;2.

Raitt, R.W., Shor, G.G., Jr., Morris, G.B., and Kirk, H.K., 1971, Mantle anisotropy in the Pacific Ocean: Tectonophysics, v. 12, p. 173–186, doi: 10.1016/0040-1951(71)90002-3.

Ribe, N., and Christensen, U., 1994, Three-dimensional modeling of plume-lithosphere interaction: Journal of Geophysical Research, v. 99, p. 669–682, doi: 10.1029/93JB02386.

Ribe, N., and Christensen, U., 1999, The dynamical origin of Hawaiian volcanism: Earth and Planetary Science Letters, v. 171, p. 517–531, doi: 10.1016/S0012-821X(99)00179-X.

Richards, M.A., Hager, B.H., and Sleep, N.H., 1988, Dynamically supported geoid highs over hotspots: Observations and theory: Journal of Geophyical Research, v. 93, p. 7690–7708.

Ritsema, J., and Allen, R.M., 2003, The elusive mantle plume: Earth and Planetary Science Letters, v. 207, p. 1–12, doi: 10.1016/S0012-821X(02)01093-2.

Ritsema, J., and van Heijst, H.J., 2000, New seismic model of the upper mantle beneath Africa: Geology, v. 28, p. 63–66, doi: 10.1130/0091-7613(2000)028<63:NSMOTU>2.3.CO;2.

Ritter, J.R.R., 2005, Small-scale mantle plumes: Imaging and geodynamic aspects, *in* Wenzel, F., ed., Perspectives in modern seismology: Heidelberg, Springer-Verlag, Lecture Notes in Earth Sciences 105: p. 69–94.

Ritter, J.R.R., Achauer, U., Christensen, U.R., and the Eifel Plume Team, 2000, The teleseismic tomography experiment in the Eifel Region, Central Europe: Design and first results: Seismological Research Letters, v. 71, p. 437–443.

Ritter, J.R.R., Jordan, M., Christensen, U.R., and Achauer, U., 2001, A mantle plume below the Eifel volcanic fields, Germany: Earth and Planetary Science Letters, v. 186, p. 7–14, doi: 10.1016/S0012-821X(01)00226-6.

Rümpker, G., and Silver, P.G., 1998, Apparent shear-wave splitting parameters in the presence of vertically varying anisotropy: Geophysical Journal International, v. 135, p. 790–800, doi: 10.1046/j.1365-246X.1998.00660.x.

Rümpker, G., and Silver, P.G., 2000, Calculating splitting parameters for plume-type anisotropic structures of the upper mantle: Geophysical Journal International, v. 143, p. 507–520, doi: 10.1046/j.1365-246X.2000.00056.x.

Rümpker, G., Tommasi, A., and Kendall, J.-M., 1999, Numerical simulations of depth-dependent anisotropy and frequency-dependent wave propagation effects: Journal of Geophysical Research, v. 104, p. 23,141–23,153, doi: 10.1029/1999JB900203.

Rümpker, G., Ryberg, T., Bock, G., and Seismology Group, D.E.S.E.R.T., 2003, Boundary-layer mantle flow under the Dead Sea transform fault inferred from seismic anisotropy: Nature, v. 425, p. 497–501, doi: 10.1038/nature01982.

Saltzer, R.L., and Humphreys, E.D., 1997, Upper mantle P wave velocity structure of the eastern Snake River Plain and its relationship to geodynamic models of the region: Journal of Geophysical Research, v. 102, p. 11,829–11,841, doi: 10.1029/97JB00211.

Saltzer, R., Gaherty, J., and Jordan, T.H., 2000, How are vertical shear wave splitting measurements affected by variations in the orientation of azimuthal anisotropy with depth?: Geophysical Journal International, v. 141, p. 374–390, doi: 10.1046/j.1365-246x.2000.00088.x.

Savage, M.K., 1999, Seismic anisotropy and mantle deformation: What have we learned from shear wave splitting?: Review of Geophysics, v. 37, p. 65–106, doi: 10.1029/98RG02075.

Savage, M.K., 2002, Seismic anisotropy and mantle deformation in the western U.S. and southwestern Canada: International Geology Review, v. 44, p. 10,913–10,937.

Savage, M.K., and Sheehan, A.F., 2000, Seismic anisotropy and mantle flow from the Great Basin to the Great Plains, western United States: Journal of Geophysical Research, v. 105, p. 13,715–13,734, doi: 10.1029/2000JB900021.

Schmid, C., Goes, S., van der Lee, S., and Giardini, D., 2002, Fate of the Cenozoic Farallon slab from a comparison of kinematic thermal modeling with tomographic images: Earth and Planetary Science Letters, v. 204, p. 17–32, doi: 10.1016/S0012-821X(02)00985-8.

Schutt, D., and Humphreys, E.D., 2001, Evidence for a deep asthenosphere beneath North America from western United States SKS splits: Geology, v. 29, p. 291–294, doi: 10.1130/0091-7613(2001)029<0291:EFADAB>2.0.CO;2.

Schutt, D., Humphreys, E.D., and Dueker, K., 1998, Anisotropy of the Yellowstone Hot Spot wake, eastern Snake River Plain, Idaho: Pure and Applied Geophysics, v. 151, p. 443–462, doi: 10.1007/s000240050122.

Sella, G.F., Dixon, T.H., and Mao, A., 2002, REVEL: A model for recent plate velocities from space geodesy: Journal of Geophysical Research, v. 107, B4, doi: 10.1029/2000JB000033.

Shen, Y., Solomon, S.C., Bjarnason, I.T., Nolet, G., Morgan, W.J., Allen, R.M., Vogfjörd, K., Jakobsdóttir, S., Stefansson, R., Julian, B.R., and Fougler, G.R., 2002, Seismic evidence for a tilted mantle plume and north-south mantle flow beneath Iceland: Earth and Planetary Science Letters, v. 197, p. 261–272, doi: 10.1016/S0012-821X(02)00494-6.

Silver, P., 1996, Seismic anisotropy beneath the continents: Probing the depths of geology: Annual Review of Earth and Planetary Science, v. 24, p. 385–432, doi: 10.1146/annurev.earth.24.1.385.

Silver, P., and Savage, M.K., 1994, The interpretation of shear-wave splitting parameters in the presence of two anisotropic layers: Geophysical Journal International, v. 119, p. 949–963.

Silver, P.G., and Chan, W.W., 1991, Shear-wave splitting and subcontinental mantle deformation: Journal of Geophysical Research, v. 96, p. 16,429–16,454.

Silver, P.G., and Holt, W.E., 2002, The mantle flow field beneath western North America: Science, v. 295, p. 1054–1057, doi: 10.1126/science.1066878.

Silver, P.G., Gao, S.S., Liu, H.K., and the Kaapvaal Seismic Group, 2001, Mantle deformation beneath southern Africa: Geophysical Research Letters, v. 28, p. 2493–2496.

Sleep, N., 1987, An analytical model for a mantle plume fed by a boundary layer: Geophysical Journal of the Royal Astronomical Society, v. 90, p. 119–128.

Sleep, N., 1990, Hotspots and mantle plumes: Some phenomenology: Journal of Geophysical Research, v. 95, p. 6715–6736.

Smith, A.D., and Lewis, C., 1999, The planet beyond the plume hypothesis: Earth-Science Reviews, v. 48, p. 135–182, doi: 10.1016/S0012-8252(99)00049-5.

Smith, G.P., and Ekström, G., 1999, A global study of P_n anisotropy beneath continents: Journal of Geophysical Research, v. 104, p. 963–980, doi: 10.1029/1998JB900021.

Song, T.A., Helmberger, D.V., and Grand, S.P., 2004, Low-velocity zone atop the 410-km seismic discontinuity in the northwestern United States: Nature, v. 427, p. 530–533, doi:10.1038,02231.

Sperner, B., Müller, B., Heidbach, O., Delvaux, D., Reinecker, J., and Fuchs, K., 2003, Tectonic stress in the Earth's crust: Advances in the world stress map project, in Nieuwland, D., ed., New insights into structural interpretation and modeling: Geological Society of London, Special Publication 212, p. 101–116.

Tommasi, A., 1998, Forward modeling of the development of seismic anisotropy in the upper mantle: Earth and Planetary Science Letters, v. 160, p. 1–18, doi: 10.1016/S0012-821X(98)00081-8.

Van der Lee, S., and Nolet, G., 1997, Upper mantle S-velocity structure of North America: Journal of Geophysical Research, v. 102, p. 22,815–22,838, doi: 10.1029/97JB01168.

Vauchez, A., Tommasi, A., Barruol, G., and Maumus, J., 2000, Upper mantle deformation and seismic anisotropy in continental rifts: Physics and Chemistry of the Earth, v. 25, p. 111–117.

Vinnik, L.P., Makeyeva, L.I., Milev, A., and Usenko, A.Yu., 1992, Global patterns of azimuthal anisotropy and deformations in the continental mantle: Geophysical Journal International, v. 11, p. 433–447.

Vinnik, L.P., Montagner, J.-P., Girardin, N., Dricker, I., and Saul, J., 2003, Comment on "Shear-wave splitting to test mantle deformation models around Hawaii" by Walker, Bokelmann, and Klemperer: Geophysical Research Letters, v. 30, p. 1675, doi: 10.1029/2002GL015751.

Walker, K.T., 2004, Exploring problems in tectonics and geodynamics with seismology [Ph.D. thesis]: Stanford, California, Stanford University, 273 p.

Walker, K.T., Bokelmann, G.H.R., and Klemperer, S.L., 2001, Shear-wave splitting to test mantle deformation models around Hawaii: Geophysical Research Letters, v. 28, p. 4319–4322, doi: 10.1029/2001GL013299.

Walker, K.T., Bokelmann, G.H.R., and Klemperer, S.L., 2003, Shear-wave splitting to test mantle deformation models around Hawaii: Reply: Geophysical Research Letters, v. 30, p. 1676, doi: 10.1029/2002GL016712.

Walker, K.T., Nyblade, A.A., Bokelmann, G.H.R., Klemperer, S.L., and Owens, T.J., 2004a, On the relationship between extension and anisotropy: Constraints from shear-wave splitting across the East African Plateau: Journal of Geophysical Research, v. 109, p. B08302, doi: 10.1029/2003JB002866.

Walker, K.T., Bokelmann, G.H.R., and Klemperer, S.L., 2004b, Shear-wave splitting reveals a mantle upwelling beneath Eastern Nevada: Earth and Planetary Science Letters, v. 222, p. 529–542, doi: 10.1016/j.epsl.2004.03.024.

Weeraratne, D.S., Forsyth, D.W., Fischer, K.M., and Nyblade, A.A., 2003, Evidence for an upper mantle plume beneath the Tanzanian craton from Rayleigh wave tomography: Journal of Geophysical Research, v. 108, 2427, doi: 10.1029/2002JB002273,2003.

Wilson, M., and Patterson, R., 2001, Intra-plate magmatism related to hot fingers in the upper mantle: Evidence from the Tertiary-Quaternary volcanic province of western and central Europe, *in* Ernst, R., and Buchan, K., eds., Mantle plumes: Their identification through time: Geological Society of America Special Paper 352, p. 37–58.

Wolfe, C.J., and Silver, P.G., 1998, Seismic anisotropy of oceanic upper mantle: Shear-wave splitting methodologies and observations: Journal of Geophysical Research, v. 103, p. 749–771, doi: 10.1029/97JB02023.

Wolfe, C.J., and Solomon, S.C., 1998, Shear-wave splitting and implications for mantle flow beneath the MELT region of the East Pacific Rise: Science, v. 280, p. 1230–1232, doi: 10.1126/science.280.5367.1230.

Wolfe, C.J., Bjarnason, J.C., VanDecar, J.C., and Solomon, S.C., 1997, Seismic structure of the Iceland mantle plume: Nature, v. 385, p. 245–247, doi: 10.1038/385245a0.

Wolfe, C.J., Vernon, F.L., III, and Al-Amri, A., 1999, Shear-wave splitting across western Saudi Arabia: The pattern of upper-mantle anisotropy at a Proterozoic shield: Geophysical Research Letters, v. 26, p. 779–782, doi: 10.1029/1999GL900056.

Wolfe, C.J., Bjarnason, G.C., VanDecar, J.C., and Solomon, S.C., 2002, Assessing the depth resolution of tomographic models of upper mantle structure beneath Iceland: Geophysical Research Letters, v. 29, 10.1029/2001GL013657.

Woodhouse, J.H., and Dziewonski, A.M., 1984, Mapping the upper mantle: 3-D modeling of Earth structure by waveform inversion: Journal of Geophysical Research, v. 89, p. 5953–5986.

Wylegalla, K., Bock, G., Gossler, J., Hanka, W., and Working Group, T.O.R., 1999, Anisotropy across the Sorgenfrei-Tornquist zone from shear wave splitting: Tectonophysics, v. 314, p. 335–350, doi: 10.1016/S0040-1951(99)00252-8.

Manuscript Accepted by the Society January 3, 2005

Printed in the USA